Final Report

Seasonal variations of black carbon in atmospheric particulate matter in lower north of Thailand

Assistant Professor Dr. Thunwadee Srithawirat

June 2018

Contract No. MRG5680112

Final Report

Seasonal variations of black carbon in atmospheric particulate matter in lower north of Thailand

Assistant Professor Dr. Thunwadee Srithawirat

Pibulsongkram Rajabhat University

Project Granted by the Thailand Research Fund

ABSTRACT

Project Code : MRG5680112

Project Title : Seasonal variations of black carbon in atmospheric particulate matter in lower north of Thailand

Investigator : Assist. Prof. Dr. Thunwadee Srithawirat

E-mail Address : T.srithawirat@psru.ac.th

Project Period : June 2013 – June 2018

Abstract : Black carbon (BC) is one of absorbing capacities of solar radiation and acts as a crucial factor that alters air quality and climate change. BC mass concentrations, associated with fine particulate matter ($PM_{2.5}$), were monitored for a year at urban and rural areas in Phitsanulok to study the seasonal variations and its contribution to fine particulate matter. The measurements were based on sampling using two simultaneously operating samplers and an optical transmissometer. $PM_{2.5}$ varied from 60.7 - 80.3 μg m^{-3} and 36.6 - 48.4 μg m^{-3} for the urban and rural sites, respectively. $PM_{2.5}$ showed similar trends with high values during dry season and low values during wet season. The BC levels during dry season ranged from 15.6 - 29.0 μg m^{-3} compared to 14.5 - 23.8 μg m^{-3} in wet season in an urban site whereas a rural site ranged from 11.1 - 15.4 μg m^{-3} and 6.8 - 13.5 μg m^{-3} for dry and wet season, respectively. The annual BC accounted for 22-38% and 19-36% in $PM_{2.5}$ at the urban and rural sites, respectively. Based on backward trajectory analysis, it can be concluded that both local and regional sources of BC are important. The local sources are traffic and biomass burning. Distant sources include areas where there is extensive agricultural burning. The model indicated the contribution of BC from the northern part of Thailand and Cambodia during days of high BC levels.

Keywords: Biomass burning, Traffic emission, Long range transport, Backward Trajectory

CONTENTS

LIST OF TABLES AND FIGURES

ACKNOWLEDGEMENTS

First, I would like to thanks to my main supervisor Prof. Dr.Peter Brimblecombe for all his help, guidance, support and experience working in the atmospheric chemistry research. I also would like to thank Assoc. Prof. Dr. Savitri Garivait and Assoc. Prof. Dr. Sirintornthep Towprayoon for all suggestions and help to complete this research. Thanks to The Joint Graduate School of Energy and Environment, King Mongkut's University of Technology Thonburi for technical help during my research work in the laboratory. Special appreciation to the Thailand Research Fund (TRF), The Office of the Higher Education Commission (OHEC) and Pibulsongkram Rajabhat University (PSRU) for sponsorship my study.

EXECUTIVE SUMMARY

Black carbon mass concentrations, associated with fine particulate matter ($PM_{2.5}$), were monitored for a year at urban and rural areas in Phitsanulok to study the seasonal variations and its contribution to fine particulate matter. The measurements were based on sampling using two simultaneously operating samplers and an optical transmissometer. The $PM_{2.5}$ concentrations were measured on the rooftop of a 4-story building at Pibulsongkram Rajabhat University. The monitoring station was located at western side of city centre (16°49'N 100°12'E). This site with an urban character is located 5 km from the national highway No.12 which is the main transport network that connects to other regions, although locally there are surrounding rice fields. A more characteristically rural sampling site is on the rooftop of a 4-story building at Sirindhorn College of Public Health, Wongthong district (16°50'N 100°23'E). This site is located approximately 40 km north of Phitsanulok and surrounded by agriculture areas. The only noticeable local source of pollution is wood burning, which is mainly carried out for cooking and sometimes to clear the forest for agricultural activity. Portable air samplers (MiniVol™ TAS 5.0, Airmetrics, USA) were used for monitoring the mass concentration of $PM_{2.5}$ at a constant flow rate of 5 L min^{-1} ± 5% with a controller for continuous measurement during the 24-h sampling period. The particles were collected on 47-mm Teflon filter paper (PTFE, Whatman, USA).

Identification of the potential impacts of different source regions on aerosol composition was assessed using backward trajectories using HYSPLIT-4 (Hybrid Single-Particle Lagrangian Integrated Trajectory) model. In this study, 72-hour-air mass trajectories ending at the sampling station were calculated with the online version of the model as a tool to determine potential backward trajectories that air crossed sampling areas at 10, 100 and 500 metres above ground level. These model runs assimilated all available observations to produce dynamically consistent six-hourly analyses and the Global Data Assimilation System (GDAS)

meteorological archive data were chosen as the input data. The backward trajectories were computed at 12:00 UTC for each sampling day.

$PM_{2.5}$ varied from 60.7 - 80.3 μg m^{-3} and 36.6 - 48.4 μg m^{-3} for the urban and rural sites, respectively. $PM_{2.5}$ showed similar trends with high values during dry season and low values during wet season. The BC levels during dry season ranged from 15.6 - 29.0 μg m^{-3} compared to 14.5 - 23.8 μg m^{-3} in wet season in an urban site whereas a rural site ranged from 11.1 - 15.4 μg m^{-3} and 6.8 - 13.5 μg m^{-3} for dry and wet season, respectively. The annual BC accounted for 22-38% and 19-36% in $PM_{2.5}$ at the urban and rural sites, respectively. Based on backward trajectory analysis, it can be concluded that both local and regional sources of BC are important. The local sources are traffic and biomass burning. Distant sources include areas where there is extensive agricultural burning. The model indicated the contribution of BC from the northern part of Thailand and Cambodia during days of high BC levels.

CHAPTER 1: INTRODUCTION

1.1 Aims of the Research

Level of scientific understanding on link between greenhouse gases and global warming is widely accepted. Scientific confidence in the relationships between emissions of CO_2, N_2O, CH_4 and fluorocarbons and temperature change is high. On the other hand, the understanding of aerosol and climate change is medium-low (IPCC, 2007). In the atmospheric aerosol, black carbon (BC) is the major absorber of visible light. BC originates from of incomplete combustion such as fossil fuels and biomass. BC has long atmospheric lifetime (i.e. several days to weeks) depending on the meteorological conditions (Babu & Moorthy, 2002) and hence are capable for long-range transport (Moorthy & Babu, 2006). Due to its strong absorption over a wide range of wavelengths, BC plays important role in the global as well as regional climate change processes, contributing significantly to the atmospheric warming (Jacobson, 2001). However, their absorption can greatly increase the earth albedo, thus cooling the planet by reducing the solar radiation reaching the surface (Schuster et al., 2005). Recent studies suggest that BC can alter the cloud lifetime (Ackerman et al., 2000), precipitation patterns (Menon et al., 2002) and report that black carbon aerosol is the second largest anthropogenic contributor to warming, adding a climate forcing about 55 percent of that of CO_2, and nearly twice that of CH_4 (Ramanathan & Feng, 2009).

Black carbon emissions generally are concentrated in South and East Asia. In Asia, these large black carbon emissions contribute to the formation of atmospheric brown clouds (ABCs) and global dimming. ABCs block sunlight by absorbing and reflecting it, both of which lead to an extensive surface dimming. The dimming effect is increased further because aerosols may nucleate more cloud droplets, which makes the clouds reflect more solar radiation (Ramanathan & Feng, 2009). The dimming has a surface cooling effect and decreases

moisture evaporation from the surface, thus slows down the hydrological cycle (Ramanathan & Feng, 2009). Chameides et al. (1999) have showed that crop yields in China are lowered because of reduced solar radiation reaching the earth. Menon et al. (2002) reported that high BC concentrations may contribute to flooding and drought in China as well as India. In view of the above, characterization of BC aerosols has assumed significance in the recent years. Despite its climate forcing potential being well accepted, large uncertainties still exist due to lack of sufficient observational data (IPCC, 2007). In addition, BC from the incomplete combustion of biomass or fossil fuels has the potential to affect both climate and health. Smith et al. (2009) reported positive significant associations of black carbon with cardiopulmonary mortality. Thus, exposure to BC is associated with a number of indicators that could contribute to cardiopulmonary deaths. However, due to lack of monitoring data, few studies have examined the adverse health effect of black carbon.

In Thailand, air pollution is one of significant environmental problems. Emissions from energy use in urban areas and biomass burning in rural areas are main factors of air pollution. Phitsanulok is located in the lower north of Thailand. As the cross-road between the northern and central regions of the country, it has long been important both for tourism and trade sectors. As a consequence, there are rapid growths of urban areas and it leads to an increase in traffic emission. Phitsanulok is also the province of agriculture. The emissions from biomass burnings of plantation for land-use change are significant environmental problems in Phitsanulok. During dry seasons (February-April), this region is affected by the plumes of smoke originating from its area and long-range transport from surrounding provinces. The biomass burning and traffic emissions release large amounts of particulates and gases, including the black carbon that may lead to an increased the global warming and climate change as well as heath impact.

In view of the above, BC is a significant part of carbonaceous aerosols from combustion which can affect on regional and global climate. Thus, the study of seasonal variations of black carbon in atmospheric particulate matter in Phitsanulok including significant

contributions of haze episodes in the northern of Thailand is important for investigating the abundances and seasonal trends of BC in atmospheric particulate matter in rural and urban sites. As aerosols will be collected both in an urban and rural location it should be possible to look at the balance of the traffic emission as compared with biomass burning emission. These forms of BC may have different toxicities so it is important to know the relative balance from a health perspective. There is a chance of examining a local health issue. Data from this project can be increased understanding of aerosol and organic chemistry in urban and agriculture regions as well as this project can be the model for other areas where affected by the haze episodes which is a significant problem for health in developing countries. The uncertainties in our understanding of the theses effects are large, but we are discovering new ways in which human activities are changing the climate and the environment. This study aims to investigate the abundances and seasonal variations of BC aerosols in rural and urban sites in Phitsanulok. Moreover, potential sources and the relative balance of BC aerosols concentration in atmospheric aerosols were also considered.

1.2 Background Knowledge

1.2.1 Atmospheric carbon definitions

Black material in smoke from wood and coal fires, has been seen as the archetypical air pollutant throughout history (Brimblecombe, 1987). Its presence in the environment even at the remotest areas was found in the 1970s and 1980s (Levin & Lindberg, 1979; Heintzenberg, 1982; Andreae, 1983), and the early studies on the environmental cycle of black carbon BC were summarized in the monograph Black Carbon in the Environment by Goldberg (1985). A recent review on the geochemistry of black carbon in the environment has been provided by Masiello (2004) and Andreae & Gelencsér (2006). Recently, the focus of black carbon study has shifted from the role as a pollutant to its importance as a driver of global warming (Andreae, 1995; Hansen et al., 1998; Hansen and Nazarenko, 2004; Hansen et al., 2005; Ramanathan et al., 2005). This atmospheric carbon has a variety of definitions

that are based on source processes, morphological characteristics, chemical composition and optical properties. Since these definitions are usually not congruent, the terminology has evolved to be confusing, complex and contradictory. In this study, the definitions for the way the various terms referring to the atmospheric carbon followed Andreae & Gelencsér (2006).

Soot: A black, blackish or brown substance formed by combustion, present in the atmosphere as fine particles (soot particles), or adhering to the sides of the chimney or pipe conveying the smoke.

Soot carbon (C_{soot}): Carbon particles with the morphological and chemical properties typical of soot particles from combustion: Aggregates of spherules made of graphene layers, consisting almost purely of carbon, with minor amounts of bound heteroelements, especially hydrogen and oxygen. This definition does not include the organic substances (oils, etc.) frequently present in or on combustion particles.

Brown carbon (C_{brown}): Light-absorbing organic matter (other than C_{soot}) in atmospheric aerosols of various origins, e.g. soil humics, humic-like substances (HULIS), tarry materials from combustion, bioaerosols, etc.

Light-absorbing carbon (LAC): General term for light absorbing carbonaceous substances in atmospheric aerosol, includes C_{soot} and C_{brown}.

Elemental carbon (EC): usually implying a near-elemental soot-carbon like composition, and in most cases referring to the fraction of carbon that is oxidized in combustion analysis above a certain temperature threshold, and only in the presence of an oxygen-containing atmosphere.

Apparent elemental carbon (EC_a): Operationally defined as the fraction of carbon that is oxidized above a certain temperature threshold in the presence of an oxygen containing atmosphere.

Black carbon (BC): generally implied to have optical properties and composition similar to soot carbon. In the climate-science community this is the most commonly used term, without consideration of its unclear definition. Also commonly used for the result of a LAC measurement by an optical absorption technique.

Equivalent black carbon (BC_e): Operationally defined as the amount of strongly light-absorbing carbon with the approximate optical properties of C_{soot} that would give the same signal in an optical instrument (e.g. the aethalometer) as the sample.

In the literature, “black carbon” or “soot carbon” are often used synonymously for the major light-absorbing component of combustion aerosols (aka “soot”) (Andreae & Gelencsér, 2006). Soot carbon has been known as an impure form of near-elemental carbon with a graphite-like structure, which is formed in flaming combustion and in combustion engines (White & Germer, 1941; Grisdale, 1953; Medalia & Rivin, 1982; Bockhorn,1994). In fact, soot particles are one of the few particle types that can be readily recognized under the scanning or transmission electron microscope by their special morphology (Oberlin, 1989). Primary soot particles, 10–50 nm spherules, do not exist by themselves in ambient air—instead they cluster together immediately after their formation in a flame to form aggregates, which are their most stable form (Wentzel et al., 2003). In fresh smoke, these clusters tend to form open structures, which are then transformed by aging processes, including the uptake of water, into more closely packed particle types (Colbeck et al., 1990; Weingartner et al., 1997; Ruellan et al., 1999; Onischuk et al., 2003). However, soot particles associated with the smoldering stage of biomass combustion usually are present as much larger spherical and compacted aggregates that seem to be more resistant to atmospheric aging processes (Martins et al., 1998).

In terms of air quality, black carbon (BC) is usually considered as a component of particles. However, a more detailed size description is often necessary and particles are often described as belonging to ultrafine, fine and coarse modes. Global, present day fossil fuel emission estimates range from 5.8 to 8.0 Tg C yr^{-1} (Haywood & Boucher, 2000; IPCC, 2007) is primarily combustion, including fossil fuel and biomass burning. BC is a major component of soot and is produced by incomplete combustion of fossil fuel and biomass (Climate and Clean Air Coalition, 2015). It is emitted from various sources including diesel cars and trucks, residential stoves, forest fires, agricultural open burning and some industrial facilities. The

main sources of black carbon include residential and commercial combustion and transport. Other important sources include industrial processes and the burning of agricultural waste. There are also small sources such as fossil fuel extraction, large scale combustion (including power plants and industrial boilers) and open burning of garbage. The BC is an important anthropogenic contribution to this load, giving 5–10% of the mass of this particulate in urban areas of US and Europe, but 10–14% of the mass over the Northern Indian Ocean (Badarinath et al., 2007). Important regional variations in emissions are expected in the coming decades, with decreases of up to half in North America and Europe due to mitigation measures in the transport sector and significant increases in Asia and Africa (Ramanathan & Crutzen, 2003).

1.2.2 Black carbon and climate change

The characterization of BC is attracting considerable interest in recent years due to its environmental and climate significance, as well as anthropogenic nature of its origin (Hansen et al., 2000). The atmospheric BC directly accounts for the reduction of the incoming short-wave solar radiation, leading to heating of the atmosphere. It has a warming impact on climate 460-1500 times stronger than CO_2 (Badarinath et al., 2009). Its lifetime varies from a few days to a few weeks. When deposited on ice and snow, BC causes both atmospheric warming and an increase of melting rate (Badarinath et al., 2009). Some model calculations suggest that its climate forcing may rival that of methane, and that the present-day global warming due to black carbon may be as much as 0.3–0.4˚C (Jacobson, 2004; Chung & Seinfeld, 2005), while others estimate a smaller climate effect from this substance (Jones et al., 2005). It also influences cloud formation and impacts regional circulation and rainfall patterns. BC is always emitted with co-pollutant particles, such as organic carbon and sulphates, which can have a neutral or even cooling effect on the climate (Ramanathan & Carmichael, 2008). The ratio of black carbon to its co-pollutants varies depending upon the emission source and fuel-type, and impacts whether the source has a net-positive or negative warming effect. For example, emissions from diesel engines have a high proportion of black carbon to cooling co-pollutants, whereas emissions from wildfires and the open-

burning of biomass contain a more balanced ratio. It is important to take the net climate effect into account when assessing black carbon emission reduction measures (Menon et al., 2002).

BC warms the climate in two ways. When suspended in air, BC absorbs sunlight and generates heat in the atmosphere, which warms the air and can affect regional cloud formation and precipitation patterns. When deposited on snow and ice, it absorbs sunlight, again generating heat, which warms both the air above and the snow and ice below, thus accelerating melting (Ramanathan & Carmichael, 2008). Because BC remains in the atmosphere for only one to four weeks, its climate effects are strongly regional. Its short lifetime also means that its climate effects would dissipate quickly if black carbon emissions were reduced, thus benefiting most directly the countries or communities that invest in policies to reduce BC emissions (Ramanathan & Carmichael, 2008). A recent study suggests that BC may be responsible for more than 30 percent of recent warming in the Arctic (Shindell & Faluvegi, 2009), contributing to the acceleration of Arctic sea ice melting. Loss of Arctic sea ice would lead to more rapid warming and possibly irreversible climate change (Field et al., 2018). BC is also driving increased melting of Himalayan glaciers, which are a major source of freshwater for millions of people in the region (Singh et al., 2011). BC may also be driving some of the observed reduction of the snowpack in the Pacific Northwest of the United States. Different types of soot contain different amounts of BC, generally the blacker the soot, the more of a warming agent it is. Fossil fuel and biofuel soot are blacker than soot from biomass burning (e.g., forest fires and wood fuel), which is generally more of a brownish color (IPCC, 2007). Based on current information, the United States is responsible for about 6% of global BC emissions; while it has a history of making reductions to improve air quality, further improvements can be made. The majority of BC emissions come from the developing world: China and India together account for some 25–35% of emissions (IPCC, 2007). Consequently, there is substantial controversy about the benefits of reducing BC as a strategy to mitigate global warming (Hansen et al., 2000; Jacobson, 2002; Bond & Sun, 2005). Because the climate effects of BC aerosol depend strongly on its

physical and chemical properties, as well as on its residence time and distribution in the atmosphere (Jacobson, 2001), a thorough understanding of these properties and accurate techniques for the determination of BC in the atmosphere are deemed essential (Andreae & Gelencsér, 2006).

Considering the key role BC plays in atmospheric radiative transfer as well as chemical properties, studies on BC aerosols have become an important topic in recent years. The studies of BC concentrations were conducted in many urban, rural, maritime and remote locations. The black smoke measurements were the earliest systematic measurements of air pollution by particulate matter (PM) in the United Kingdom (Brimblecombe, 1987), and the method has been used in many European countries (e.g. Hoek et al., 2002). The BC concentrations were detected in Houston, USA and over the Pacific, and even in the Antarctic (e.g. Schwarz et al., 2009, 2010; McMeeking et al., 2010). Zhao et al., (2012) reported BC background concentration near the Glacier in north western China varied in the range of 18–72 ng m^{-3} with the highest in summer and the lowest in autumn. In background sites in Finland, BC ranged from 60-460 ng m^{-3}. The report from Kumar (2011) showed that the annual average BC mass concentration at Anantapur, India is 1.97± 0.12 μg m^{-3}. Seasonal variations of BC aerosol mass concentration showed high during the dry (winter and summer) seasons and low during the post-monsoon followed by the monsoon seasons. In Austria, previous studies showed that BC concentrations can reach up to 40 μg m^{-3} in Vienna under polluted conditions in winter, while in summer concentrations are lower (<10 μg m^{-3}, Hitzenberger et al., 1996). Husain et al. (2007) recently reported BC concentrations in urban of Lahore, Pakistan from November 2005 to January 2006 were very high, ranging from about 5-110 μg m^{-3}. During the Indian Ocean Experiment (INDOEX), Mayol-Bracero et al. (2002) reported mean BC concentrations of 3200 ng m^{-3} in the residual continental boundary layer over the Northern Indian Ocean which formed about 14% of the total aerosol. Studies during ACE-Asia have indicated the presence of BC (200-1800 ng m^{-3}) at below 3 km altitude over the East Asian region (Mader et al., 2002).

In Thailand, few studies of BC concentrations have been reported scientific literature. Kanokkanjana et al. (2011) presented amount of BC emission from open burning of rice residues in Thailand. Emission factor results of BC from open burning experiment in the chamber are 0.79 ± 0.36 gBC/kg_{dm} from rain-fed rice residues burning and 0.72 ± 0.03 gBC/kg_{dm} from irrigated rice residues burning. Measurements of BC and EC were performed at different locations across Asia and the South Pacific in both urban and suburban locations in Australia, Bangladesh, India, Korea, Malaysia, Mongolia, New Zealand and Thailand during the winter of 2007 to the winter of 2010 (Salako et al., 2012). The overall average concentrations of EC and BC were calculated as 6.21 μg m^{-3} and 7.29 μg m^{-3}, respectively. The lowest relationships between BC and EC concentrations were found for the two Bangkok, Thailand sites. The highest correlations were found for the samples collected in Bangladesh and in New Zealand (Salako et al., 2012).

The climate effects of BC aerosol depend strongly on its physical and chemical properties as well as on its residing time and distribution in the atmosphere (Jacobson, 2001). Global warming due to black carbon may be as much as 0.3-0.4 $^{\circ}C$ (Jacobson, 2004; Chung & Seinfeld, 2005) whiles others estimating a smaller climate effect from it (Jones et al., 2005). It has also been mentioned that carbon containing particles contaminates building materials (Ghedini et al., 2000) and adversely impact terrestrial and aquatic ecosystems (Forbes et al., 2006). It has also been observed the impacts of BC on Tibetan Plateau and thereby on the Asian hydrological cycle and monsoon climate (Qian et al., 2011). All these adverse effects of black carbon on the human and climate including their increasing concentration in developing countries are making the scientific communities study in detail, its source, its physical and chemical properties and its detrimental impacts on nature.

1.2.3 Black carbon measurement

Black carbon is produced by incomplete combustion of carbonaceous fuels. It is a unique primary tracer for combustion emissions, as it has no non-combustion sources, and is stable once released into the atmosphere. It absorbs light in the visible part of the spectrum, which

is the basis of its detection. It is composed of chains of agglomerated graphitic spheres with particles having aerodynamic diameters between 10 and 200 nm (Invernizzi, et al., 2011). Measurements of airborne black carbon are aimed at estimating the concentration of airborne elemental carbon by the absorption of light passing through PM collected on a filter (Quincey, 2007). There are two prevailing filter-based methods for collecting BC data on a large scale: optically based real-time BC monitoring methods (such as the Aethalomete) which utilize light-absorbing characteristic of BC aerosols for measurement (Hansen et al., 1984); and thermal-optical methods (destructive thermal evolution techniques) which utilize thermal and chemical refractory properties for measurement of BC samples collected over a period of several hours (Chow et al., 1993).

There are several types of measurement method and commercial instrument available for continuous, semi-continuous and integrated filter sample-based optical and thermal-optical measurements of aerosol parameters reflecting combustion-derived char, soot, black carbon or elemental carbon contents in PM. The concentrations of these carbonaceous material are low or moderate (close to source) in atmospheric PM, and much higher in emissions from common combustion sources (diesel engines, power plants or ship engines using heavy oil, or small residential heaters using wood or other biomass). A thermal optical reflectance method can be applied to differentiate between char-EC and soot-EC according to a stepwise thermal evolutional oxidation of different proportions of carbon under different temperatures and atmosphere. Taking into account the wide variations in the formation and composition of combustion-derived PM, and the fact that some of its chemical composition is known to exert not only light-absorbing (soot/BC/EC) but also considerable light-scattering (organics, inorganics) properties, it is no surprise that many indirect optical measurement techniques and thermal optical analysis methods, which have been used for many years in air quality measurements by aerosol and by health scientists, have proved to give only a rough proxy of the BC or EC concentration in ambient air without instrument-specific corrective measures. Some methods have also had instrument-specific technical problems during operation in large methodological inter-comparison studies conducted by the leading

aerosol scientists in Asia, Europe and the United States (Müller et al., 2011; Chow et al., 2009; Reisinger et al., 2008; Kanaya et al., 2008; Hitzenberger et al., 2006).

Combustion-derived soot and char (in practice, their dark components) have been determined in epidemiological studies by the following techniques: light reflectance from (absorbance (Abs), BS) or light transmission through (basis of measurement of BC) integrated PM samples usually collected at 24-hour intervals on thin cellulose fiber filter or other filter material, followed by conversion of the optical measurement units to mass-based units; real-time photometers measuring light absorption of PM sample spots (BC) at 1–5 minute intervals and automatically giving readings in mass-based units; chemical determination of EC and organic carbon (OC) using thermal optical analysis methods either semi-continuously with mass-based readings given every 30 minutes to 3 hours, or from integrated PM samples collected at 24-hour intervals on quartz filters (Müller et al., 2011; Janssen et al., 2011; Chow et al., 2009).

The absorption coefficient of PM and BS measured with a reflectometer and BC measured with an optical transmissometer are metrics that are based on the blackness of aerosol material collected on a filter. Light is focused on the filter sample and the amount of light reflected or transmitted is measured. For BS and Abs, the amount of reflected light is converted into PM mass units (OECD standard) (OECD, 1964) or the black smoke index ISO standard 9835:1993 (ISO, 1993), whereas in the BC method the light transmitted is converted to represent the mass of EC. BS measurement has been used in Europe since the 1920s, when urban air pollution was dominated in many places by smoke from coal combustion. Although BS and Abs determinations are expressed in $\mu g\ m^{-3}$, there is no clear relationship to PM mass, as conversion of the optical measurement results into mass units depends on location, season and type of combustion particle. Absorption photometers for real-time application have been available since the 1980s. These are filter-based instruments that measure at intervals of one to five minutes the changes in transmittance through a fibrous filter tape as particles are deposited. The complex relationship between changes in

light transmission and aerosol absorption and scattering on the filter requires an adequate calibration of these methods, including the selection of an effective wavelength for a valid absorption co-efficient, determination of filter spot size and characterization of the aerosol flow (Müller et al., 2011). Algorithms have been published for correcting artefactual enhancement of light absorption by filter-loading, back-scattering, and multiple scattering caused by PM and the filter matrix in connection with aethalometers and particle soot absorption photometers. The multi-angle absorption photometer is the only real-time absorption photometer that corrects for these artefacts by design (Müller et al., 2011; Chow et al., 2009).

Thermal optical methods are based on OC and EC removed from sampling substrates (such as quartz-fiber filter) by volatilization and/or combustion at selected temperatures, and by conversion of the released gases to carbon dioxide (CO_2) or methane (CH_4). This is followed by infrared absorption (CO_2) or flame ionization (CH_4) detection. EC is not volatile and is only released by oxidation. Most of the atmospheric OC tends to evolve at temperatures $\leq$ 550°C in pure helium atmosphere and, thus, it can be separated from EC that needs to be oxidized in helium 98%/oxygen 2% at temperatures $\geq$ 550°C. Heating in an inert helium atmosphere, however, causes certain OC compounds to pyrolyse or char, thereby exaggerating the atmospheric EC in the sample. In thermal optical carbon analysis, this can be corrected by simultaneous measurement of thermal optical reflectance (TOR) or thermal optical transmittance (TOT). Although the principles of thermal methods appear to be similar, they contain variations with respect to: location of the temperature monitor (thermocouple) relative to the sample, analysis atmospheres and temperature ramping rates; temperature plateaus; residence time at each plateau; optical pyrolysis monitoring configuration; carrier gas flow through or across the sample; and oven flushing conditions. Chow et al. (2005; 2009) and Han et al. (2007; 2010) have done a lot of development and comparisons of thermal optical methods. Currently, their Interagency Monitoring of Protected Visual Environments (IMPROVE_A) thermal optical reflectance protocol (IMPROVE_A_TOR) seems

the best thermal optical method for separating various OC fractions from each other as well as for separating char-EC from soot-EC.

Comparison of the optical measurement methods with each other and with more sophisticated methods BS/PM_{10} ratios measured with the reflectometer have varied widely in Europe and many times exceeded one in some locations (Hoek et al., 1997), as the Abs units are converted to BS values in μg m^{-3} by using a constant conversion factor. This is a major source of bias, because the greatly varying OC/EC ratio in PM affects Abs due to scattering of light from combustion-type organic material. A typical OC/EC ratio in urban traffic environments is two, while the OC/EC ratio can be five in rural background areas with more prevalent biomass combustion. Thus, BS data from different types of site or from different seasons or from decade-long time-series at the same site are not comparable. BS measurement should always be accompanied by local calibration of the conversion factor from Abs units to BS values in μg m^{-3} on the basis of the OC/EC ratio in PM (Schaap & Denier van der Gon, 2007).

The variability in the chemical composition of BC aerosol at different locations also biases the BC data of optical transmissometers. It has been suggested that these should be calibrated with the help of more sophisticated and reliable measurement techniques using statistically significant numbers of samples for the specific sites (Ahmed et al., 2009). As with reflectometers, however, controlling the measurement bias by local calibrations may not be easy, because the OC/EC ratio in PM can also vary with the season and with day-to-day temperatures at the same site due to variations in biomass combustion for residential heating. Aerosol scientists have produced valuable information about the type and quantity of sources of measurement error in relation to absorption photometers for real-time application (Müller et al., 2011; Chow et al., 2009; Reisinger et al., 2008; Kanaya et al., 2008; Hitzenberger et al., 2006). In fact, the use of filter-based instruments to derive information on aerosol light Abs and BC is a matter of debate (Müller et al., 2011), as is the use of older optical measurements of BS and Abs (see Janssen et al., 2011). Currently, there is no

generally accepted standard method to measure BC or EC. It has, however, been possible to make comparisons of several filter-based instruments of aerosol light Abs with more sophisticated instruments such as the photoacoustic analyzer (Chow et al., 2009).

1.2.4 Health effects of black carbon

The health effects of combustion-related air pollution indicated by black particles were identified decades ago, when the monitoring of black smoke (or "British smoke" – BS) was a widespread method for air quality assessment in Europe. The evidence about the health effects of this pollution was used to recommend the first guidelines for exposure limits (then) consistent with the protection of public health (WHO, 1979). In the 1990s, BS was one of the indicators of air quality used, for example, in European time-series studies linking mortality with pollution (Katsouyanni et al., 2001). A recognition of the difficulties in standardizing BS measurements and an appreciation of the health effects of the non-black components of particulate matter (PM) attracted the attention of researchers and regulators to the mass concentration of inhalable or respirable fractions of suspended PM such as PM_{10} and $PM_{2.5}$ (WHO, 2000). Black carbon and co-pollutants make up the majority of $PM_{2.5}$ air pollution, and is the leading environmental cause of poor health and premature death. In 2010, household $PM_{2.5}$ air pollution and ambient outdoor $PM_{2.5}$ air pollution were estimated to have caused over 3.5 and 3.2 million premature deaths, respectively (Lin et al. 2011). BC causes serious health problems as it can get easily deposited into the respiratory system through inhalation because of its fine submicron size. Recently, BC has been used as an indicator of exposure to diesel soot (e.g. Fruin et al., 2004), which has been classified as a toxic air contaminant and a suspected carcinogen. In a meta analysis of existing time-series studies of black carbon and daily mortality, most of which were conducted in North America and Europe, Smith et al. (2009) reported positive significant associations of black carbon with cardiopulmonary mortality. Several previous studies support the biological plausibility of a link between exposure to black carbon and exacerbations of cardiopulmonary disorders (Gold et al., 2005; Henneberger et al., 2005; Mar et al., 2005). For instance, one study in Germany examined weekly electrocardiograms of 56 men with a history of heart disease, and found

significant associations of black carbon with changes in myocardial repolarization, which could increase the risk of sudden cardiac death (Henneberger et al., 2005). Gold et al. (2005) found associations of black carbon with ST-segment depression among a panel of 24 elderly Boston residents. Exposure to black carbon was also associated with increased nitric oxide in exhaled breath, a marker of airway inflammation (Mar et al., 2005). Thus, exposure to black carbon is associated with a number of indicators that could contribute to cardiopulmonary deaths. However, due to lack of monitoring data in Asia, few studies have examined the adverse health effect of black carbon in China (Lin et al., 2011). Grahame & Schlesinger (2010) reviewed the evidence of the effects of BC on cardiovascular health endpoints and concluded that it may be desirable to promulgate a BC $PM_{2.5}$ standard. Conversely, Smith et al. (2009) noted that although the results of their time-series meta-analysis suggest greater effects per unit mass of sulfate than BS, this distinction was less clear in the few studies that directly compared the estimated effects of both indicators. This indicates the need for a critical comparison of studies that have measured PM mass as well as BC particles.

The light Abs of $PM_{2.5}$ filter samples has been used in most European epidemiological studies as a measure of exposure to black carbon particles (BCP), whereas in studies in the United States, the EC content of the samples has mostly been used for the purpose. In some studies, Abs has been further converted into BS, which was widely used in the past in Europe for air quality monitoring. However, the conversion factor found in ISO standard 9835:1993 (ISO, 1993) is not suitable for present-day particulate air pollution mixture, but local calibration factors should be used. In earlier studies, the coefficient of haze may have been used as a measure of BCP. Because of similar measurement principles, the method gives results that are highly correlated with BC concentrations obtained with more modern methods such as aethalometers. Real-time BC measurement methods will undoubtedly increase in popularity with time, especially in settings where filter sampling is not needed for other purposes.

Time-series study design has been the most frequently used method to evaluate the acute effects of BC exposure on population health. The design is based on comparing short-term (typically daily) variations in exposure with short-term variations in population health, for example, mortality or hospitalization. In the setting, population exposure is assessed by measuring BCP at one or more centrally located outdoor monitoring stations. The accuracy of estimates of the effects on health eventually depends on how well daily BCP levels measured at the central outdoor monitoring site (ambient BCP) reflect daily changes in personal exposure to BCP (personal BCP) in the study area. It should be noted that ambient concentration is a valid proxy for personal exposure even when an individual's exposure on a given day may not be predicted very accurately because of random error (Zeger et al., 2000). In contrast, an inability by outdoor monitoring to reflect daily mean exposure in the study population leads to biased health effect estimates. Panel studies with repeated clinical and air pollution measurements similarly rely on accurate assessment of day-to-day variability in exposure.

Outdoor BCP has also been found to be more strongly associated with respective indoor levels than $PM_{2.5}$ in cross-sectional studies (Gotschi et al., 2002). It should be noted that there are substantial differences in infiltration rates between geographical areas due to differences in building codes and human behaviour, and thus generalizability of the results from single (-city) studies is limited. In the absence of indoor sources, indoor/outdoor concentration ratios can be interpreted to reflect infiltration directly. The effect of indoor sources can be eliminated by taking measurements at night or in an uninhabited building. Such studies have also reported higher infiltration for BCP than for $PM_{2.5}$: 0.84 versus 0.48 in Los Angeles homes (Sarnat et al., 2006), and 0.61 versus 0.41 for a home in Clovis, California (Lunden et al., 2008). Concentrations measured at a central outdoor site have been found to reflect well temporal variability in 24-hour concentrations of both $PM_{2.5}$ and BC across urban areas (Puustinen et al., 2007). Considering that BCP and $PM_{2.5}$ do not seem to differ in that respect, the higher infiltration rate for BCP may be the main reason for the observed higher ambient—personal correlation for BCP. Overall, measurement errors for

BCP and $PM_{2.5}$ seem comparable, which means that effect estimates obtained in epidemiological studies for the two can be directly compared. Even hourly peak exposures may be relevant to health as potential triggers of cardiorespiratory events. Although ambient 24-hour levels of BCP seem to reflect personal exposures well, it can be assumed that the correlation is lower on shorter time-scales due to short-term changes in ventilation (for example, opening windows at home or in a car) and the microenvironment (such as an office or in a public transport vehicle). Short-term BCP exposures are noticeably elevated during commuting (Adams et al., 2002), and the differences between background concentrations and concentrations measured in traffic by cyclists and passengers in vehicles seem to be even greater for BCP than for $PM_{2.5}$ (Zuurbier et al., 2010). BCP also has significant indoor sources, such as cooking and environmental tobacco smoke, which may lead to peaks in exposure (Lanki et al., 2007; Raaschou-Nielsen et al., 2011). A reasonable assumption is that these indoor sources do not confound the association between ambient BCP and health outcomes because the strength of the source is not related to ambient levels. Distinguishing between the effects of highly correlated air pollutants is always challenging because of potential problems caused by multi-collinearity in statistical models. Daily variations in BCP in urban areas are most strongly associated with local traffic emissions (Vallius et al., 2005), although factors such as long-range transported air pollution, local industry, open biomass burning, and residential wood and coal combustion may also affect the concentrations (Larson et al., 2004).

1.3 Key Aims of the Research

To investigate the abundances and seasonal variations of BC aerosols in rural and urban sites in Phitsanulok

To explore potential sources of BC aerosols

To compare the relative balance of BC aerosols in rural and urban sites

CHAPTER 2: METHODOLOGY

2.1 Experimental site

Phitsanulok province of lower north of Thailand with an area of 10,816 km² and a population of 863,404 and includes the city of Phitsanulok (Population: ~180,000). The climate of Phitsanulok is influenced by monsoon winds and has a seasonal character with a dry (May–October) and wet season each year. The south-west monsoon brings a stream of warm moist air from the Indian Ocean causing abundant rain over the country with temperatures ranging from 21 to 37 °C and relative humidity from 61 to 80%. The north-east monsoon (October–February) brings the cold and dry air that derives from anticyclonic conditions on the Chinese mainland with temperatures ranging from 18 to 33 °C and relative humidity from 62 to 78% (TMD, 2013).

2.2 Sample collection

$PM_{2.5}$ (particulate matter with an aerodynamic diameter of less than 2.5 micrometers) concentrations were measured on the rooftop of a 4-story building at Pibulsongkram Rajabhat University (Fig. 1, S1). The monitoring station was located at western side of city centre (16°49'N 100°12'E). This site with an urban character is located 5 km from the national highway No.12 which is the main transport network that connects to other regions, although locally there are surrounding rice fields. A more characteristically rural sampling site is on the rooftop of a 4-story building at Sirindhorn College of Public Health (Fig. 1, S2), Wongthong district (16°50'N 100°23'E). This site is located approximately 40 km north of Phitsanulok and surrounded by agriculture areas. The only noticeable local source of pollution is wood burning, which is mainly carried out for cooking and sometimes to clear the forest for agricultural activity.

Portable air samplers (MiniVol™ TAS 5.0, Airmetrics, USA) were used for monitoring the mass concentration of $PM_{2.5}$ at a constant flow rate of 5 L min^{-1} ± 5% with a controller for continuous measurement during the 24-h sampling period. The particles were collected on 47-mm Teflon filter paper (PTFE, Whatman, USA). Before and after sampling, the filters were stored in desiccators for 24 h prior to an initial weighing in a clean room under controlled temperature and relative humidity conditions. The sampling was undertaken 1.5 m away from the boundary of the buildings. The device was placed at a height of 10 m from the ground. A total of 120 samples were collected from each sampling site for 10 days a month on randomly selected days during November 2013 to October 2014. The total mass of the filter paper was calculated by the gravimetric method. The Teflon filters were first equilibrated in a clean room that maintains the inner chamber under the required conditions, at 60% relative humidity and 25°C for a minimum of 24 hours. Typically, the relative humidity varied by less than 2%, and temperature by less than 1°C in this room. After equilibration, mass measurements were then made using a micro analytical balance (MC5, Sartorius, USA). The balance has a readability of 1 µg with an average response time of approximately 10 seconds. Each sample was weighed a minimum of three times to ensure adequate precision. Ten percent of the samples were re-weighed as new samples as a quality assurance check. After collecting, the filters were refrigerated at about 4 °C prior to chemical analysis.

2.3 Black carbon measurement

BC was measured in the filters of $PM_{2.5}$ mass. The filter samples were equilibrated for 24 hours to remove particle-bound water. However, some water can remain associated with the particles after equilibration. The sample collected on a filter was loaded onto a dual-wavelength optical transmissometer (SootScan OT21, Magee Scientific, USA) to measure BC. The optical transmissometer measures and compares the transmission intensity of light at 880 and 370 nm passing through an exposed filter with that of a blank, unexposed filter. Thus, as to determine the attenuation ATN (ATN = -ln(T/To), where T and To are the respective transmission intensities through the loaded and blank filters). Optically based methods assume that ATN through the filter is proportional to the BC loading on the filter

paper (Hansen et al., 1984; Liousse et al., 1993; Petzold et al., 1997). Five replicate measurements were collected for each sample filter spot. Each measurement provides an ultraviolet (UV) and infrared (IR) attenuation by the particles present on a filter spot. Based on the average IR and UV attenuation, area of the filter exposed for particle collection (in cm^2) and the volume of air sampled (in cubic meters), we can calculate the concentration of BC and UVBC in μg m^{-3}. This system provides measurements that are highly correlated with concentrations measured using the National Institute for Occupational Safety and Health (NIOSH) thermal–optical method (Ahmed et al., 2009). Analytical uncertainty and limit of detection (LOD) of the instrument were 1.73% and 0.14 μg m^{-3}.

2.4 Air mass trajectories

Identification of the potential impacts of different source regions on aerosol composition was assessed using backward trajectories using HYSPLIT-4 (Hybrid Single-Particle Lagrangian Integrated Trajectory) model. The HYSPLIT model is a complete system for computing simple air parcel trajectories to complex dispersion and deposition simulations (Stein et al., 2015). In this study, 72-hour-air mass trajectories ending at the sampling station were calculated with the online version of the model as a tool to determine potential backward trajectories that air crossed sampling areas at 10, 100 and 500 metres above ground level. These model runs assimilated all available observations to produce dynamically consistent six-hourly analyses and the Global Data Assimilation System (GDAS) meteorological archive data were chosen as the input data. The backward trajectories were computed at 12:00 UTC for each sampling day.

2.5 Statistical analyses

Analysis of the experimental data was performed using the Statistical Package for Social Sciences (SPSS Version 11.5, IBM, USA). Descriptive statistics, including the mean, standard deviations, minimum, maximum and median were used to investigate the concentrations of the $PM_{2.5}$ and black carbon samples. The significance of the difference

among $PM_{2.5}$ and black carbon concentration in dry and wet season from two sampling were evaluated by Chi-square test. Pearson correlation coefficients were used to evaluate the relationship of the black carbon concentrations between hotspots.

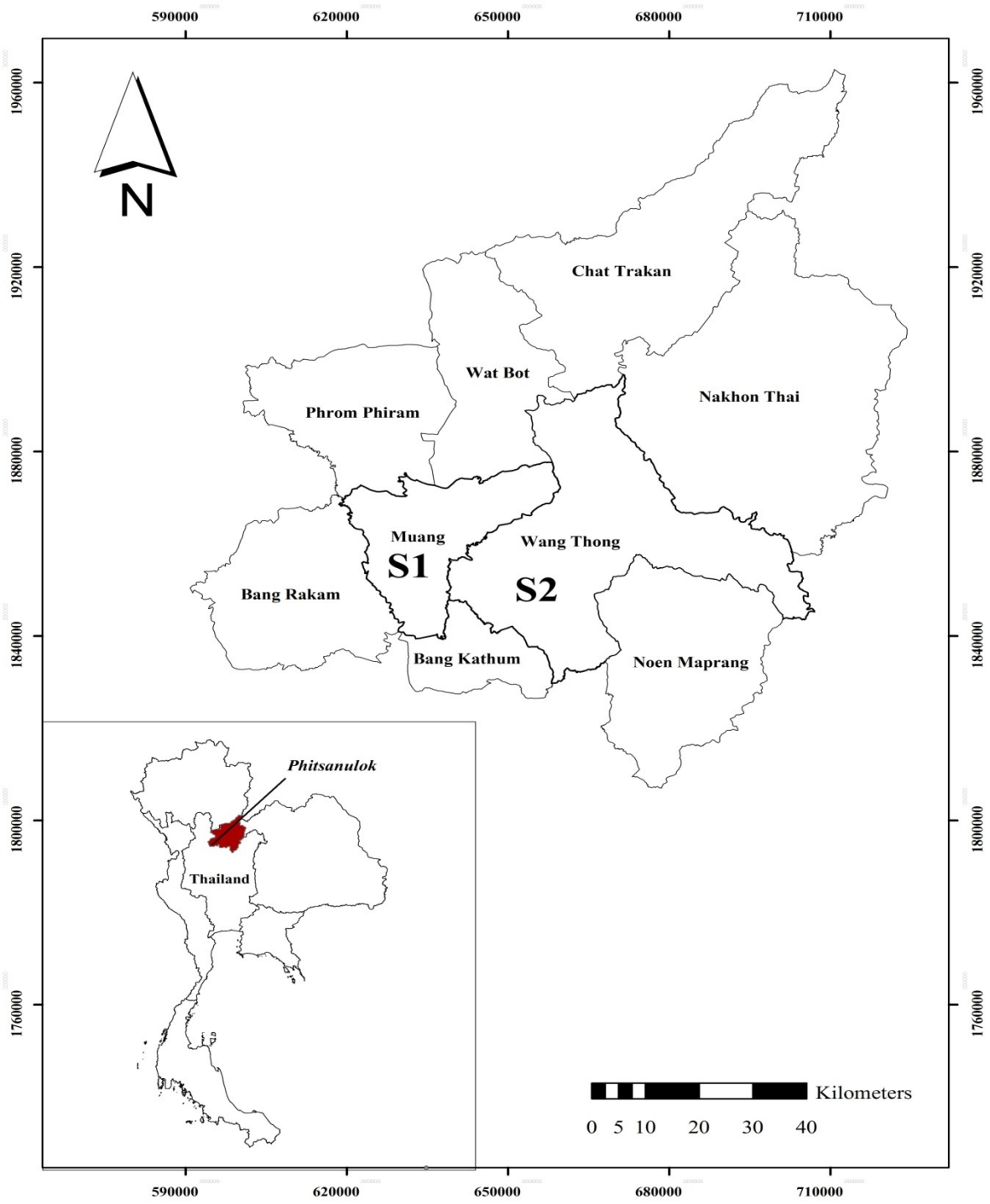

Fig. 1 Location of the sampling site at Phitsanulok, Thailand

CHAPTER 3: RESULTS AND DISCUSSION

3.1 Seasonal variation of $PM_{2.5}$

During the study period the levels of $PM_{2.5}$ at the urban site varied from 60.7 to 80.3 μg m^{-3} with a mean of 69.6 ± 8.6 μg m^{-3}. For the rural site, $PM_{2.5}$ levels ranged from 36.6 to 48.4 μg m^{-3} with a mean of 42.4 ± 5.6 μg m^{-3}. The monthly variations of $PM_{2.5}$ during the study period are presented as Box-Whisker plots in Fig. 2. The yearly average value of the urban site (69.6 μg m^{-3}) for $PM_{2.5}$ mass during the study period is much higher than the yearly average concentration of Thai National Ambient standard (25 μg m^{-3}) as well as USEPA standard.

Plots of both $PM_{2.5}$ in urban and rural sites showed similar trends with high values during dry season (46.8-79.8 μg m^{-3}) and low values during wet season (36.1-61.9 μg m^{-3}). This is because PM is removed by wet deposition as Phitsanulok receives high rainfall (annual average value of 1470 mm). This wet deposition is an important process in removing PM and other pollutants from the atmosphere under favorable climatic conditions, i.e., a combination of precipitation amount and intensity (Guo et al., 2014). The concentrations of $PM_{2.5}$ in urban site were significantly higher during the dry season compared to the wet season, and the concentrations were significantly different in rural site ($p < 0.05$) when excluding the fluctuations found in May 2014. Not surprisingly the mean $PM_{2.5}$ concentration of the urban site was significantly higher than those of the rural site ($p < 0.05$), probably the result of local activities such as traffic flow and open burning.

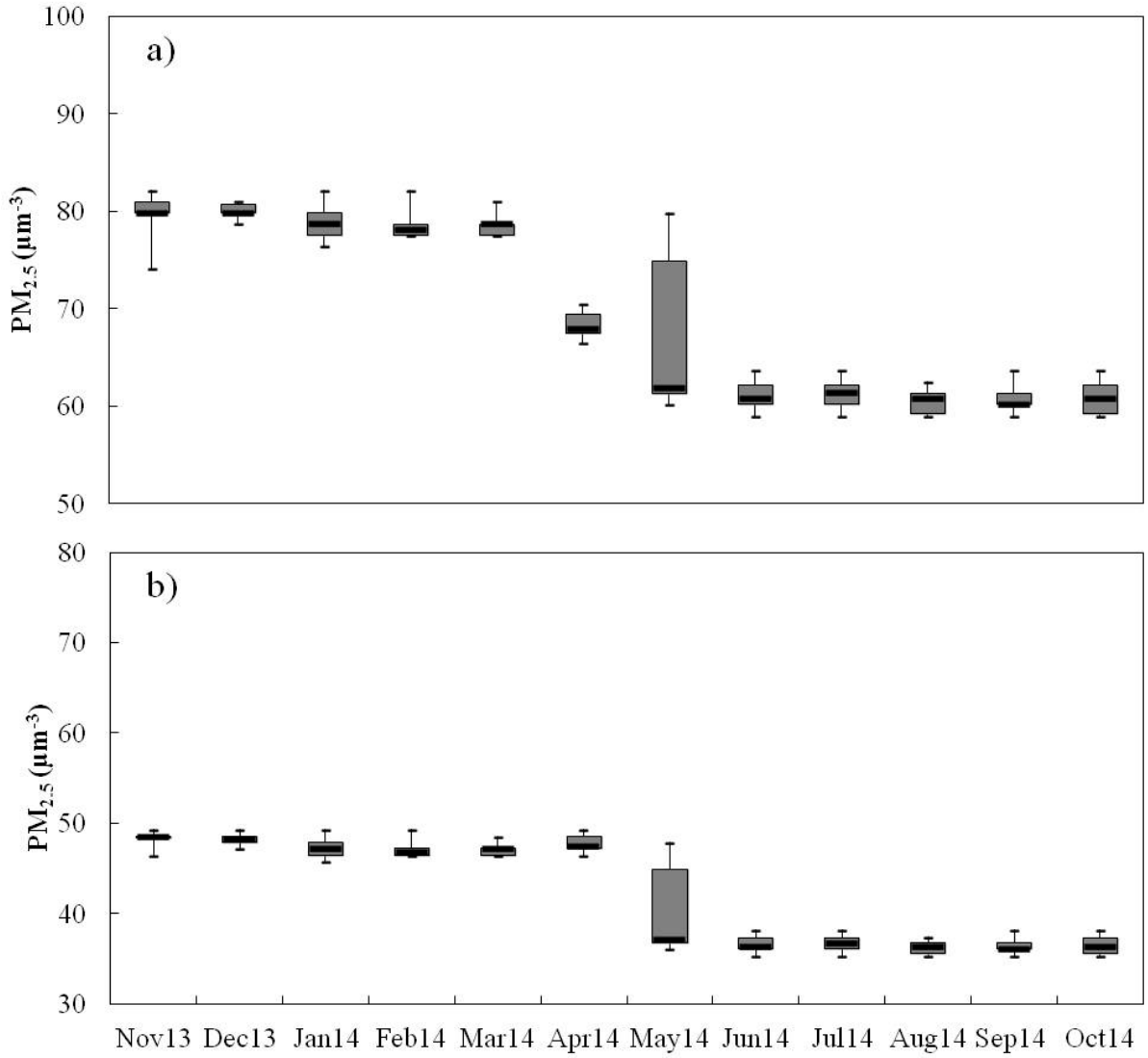

Fig. 2 Seasonal variation of $PM_{2.5}$ (a) urban site (b) rural site. The box represents 25–75% whereas the whiskers represent the upper 25% and lower 25% of the distributions of the monthly $PM_{2.5}$ concentration. The horizontal line in the box indicates the median of the distribution for the month.

3.2 Seasonal variation of black carbon (BC)

The Box-Whisker plot of BC levels in $PM_{2.5}$ measured during the study period was presented in Fig. 3. The plot shows similar annual cycles with higher BC values during dry season (December 2013 – February 2014) compared to wet season in both of urban and rural sites. For the urban site, the BC levels during dry season ranged from 15.6 to 29.0 μg m^{-3} compared to 14.5 to 23.8 μg m^{-3} in wet season. Concentrations of BC observed at the rural site ranged from 11.1 to 15.4 μg m^{-3} and from 6.8 to 13.5 μg m^{-3} for dry and wet seasons, respectively. However, the average concentrations showed significant differences between dry and wet seasons of both sites ($p < 0.05$). The annual variation of BC is important because it aids the estimation of regional radiative impacts with increased accuracy (Babu & Moorthy, 2002). A previous study of Chen et al. (2001) did not find any significant annual variations, whereas a study of Babu & Moorthy (2002) showed strong annual variation with a maximum to minimum ratio > 3. As the measurement locations are not affected by industrial activities, the BC concentrations can be affected by seasonal anthropogenic activities. The observed seasonal changes would be primarily associated with the synoptic meteorology and long range transport such as atmospheric circulation, the emission sources on the upwind side, and/or precipitation along the transport pathway (Babu & Moorthy, 2002 ; Wang et al., 2016).

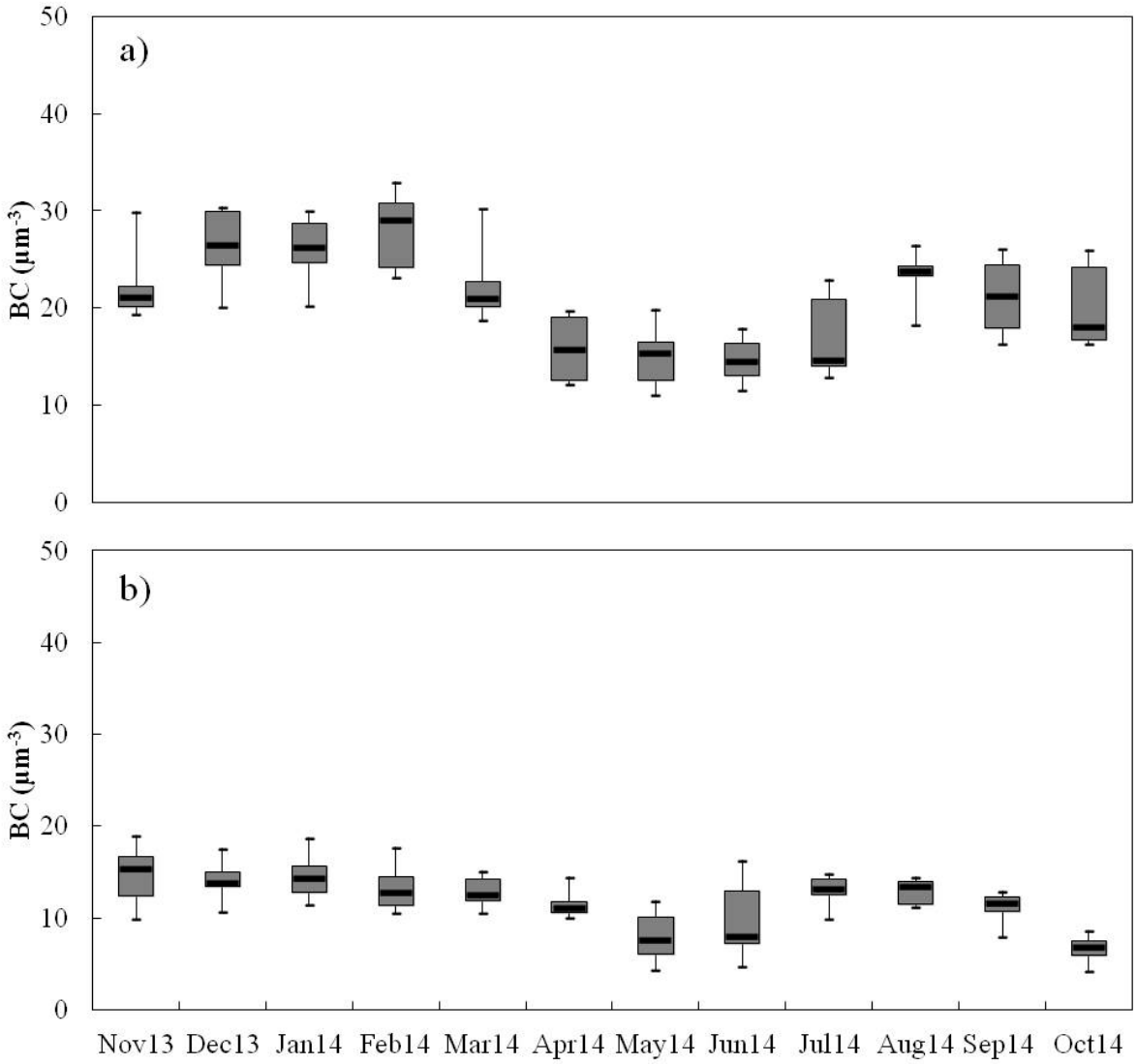

Fig. 3 Seasonal variation of BC (a) urban site (b) rural site. The box represents 25–75% whereas the whiskers represent the upper 25% and lower 25% of the distributions of the monthly $PM_{2.5}$ concentration. The horizontal line in the box indicates the median of the distribution for the month.

Black carbon contributes about 19-36% of the mass of $PM_{2.5}$ at the rural site, whereas the concentrations of BC in $PM_{2.5}$ at the urban site represented about 22-38% of the $PM_{2.5}$. These values were similar to the observed at the proportion of BC to $PM_{2.5}$ (27%) at a roadside in Hong Kong (Cao et al., 2006), but slightly lower than that (43%) observed at an urban roadside in Paris (Ruellan & Cachier, 2001). These high contributions of BC to $PM_{2.5}$ can be attributed to the proximity to major roads. A lower proportion (an average of 8%) was reported in a suburban area of Xi'an, China (Cao et al., 2009) and an urban area of Beijing, China (an average of 7%) (Chen et al., 2016), mainly because of the decreasing contribution of traffic. Monthly BC to $PM_{2.5}$ mass ratio is shown in Fig.4. For the urban site, the ratio during dry season ranged from 0.2 to 0.4 compared to 0.1 to 0.4 in wet season. BC to $PM_{2.5}$ ratio observed at the rural site ranged from 0.2 to 0.4 and from 0.1 to 0.5 for dry and wet seasons, respectively.

Black carbon is widely viewed as an indicator of diesel engine vehicle emissions in areas of dense traffic (Zhu et al., 2002; Wang et al., 2009). In Phitsanulok, all buses and trucks are equipped with diesel engines, whereas motorcycles and passenger cars mostly use gasoline engines. The $PM_{2.5}$ concentration was found to correlate closely with BC concentration at urban site (R = 0.48, p < 0.01, N = 120) and rural site (R = 0.47, p < 0.01, N = 120). For seasonal comparison, the highest correlation between BC and $PM_{2.5}$ was found at urban site during dry season was high (R = 0.63, p < 0.01, N = 60). The good correlation between the BC and $PM_{2.5}$ also suggests that the $PM_{2.5}$ was a better indicator of local emissions.

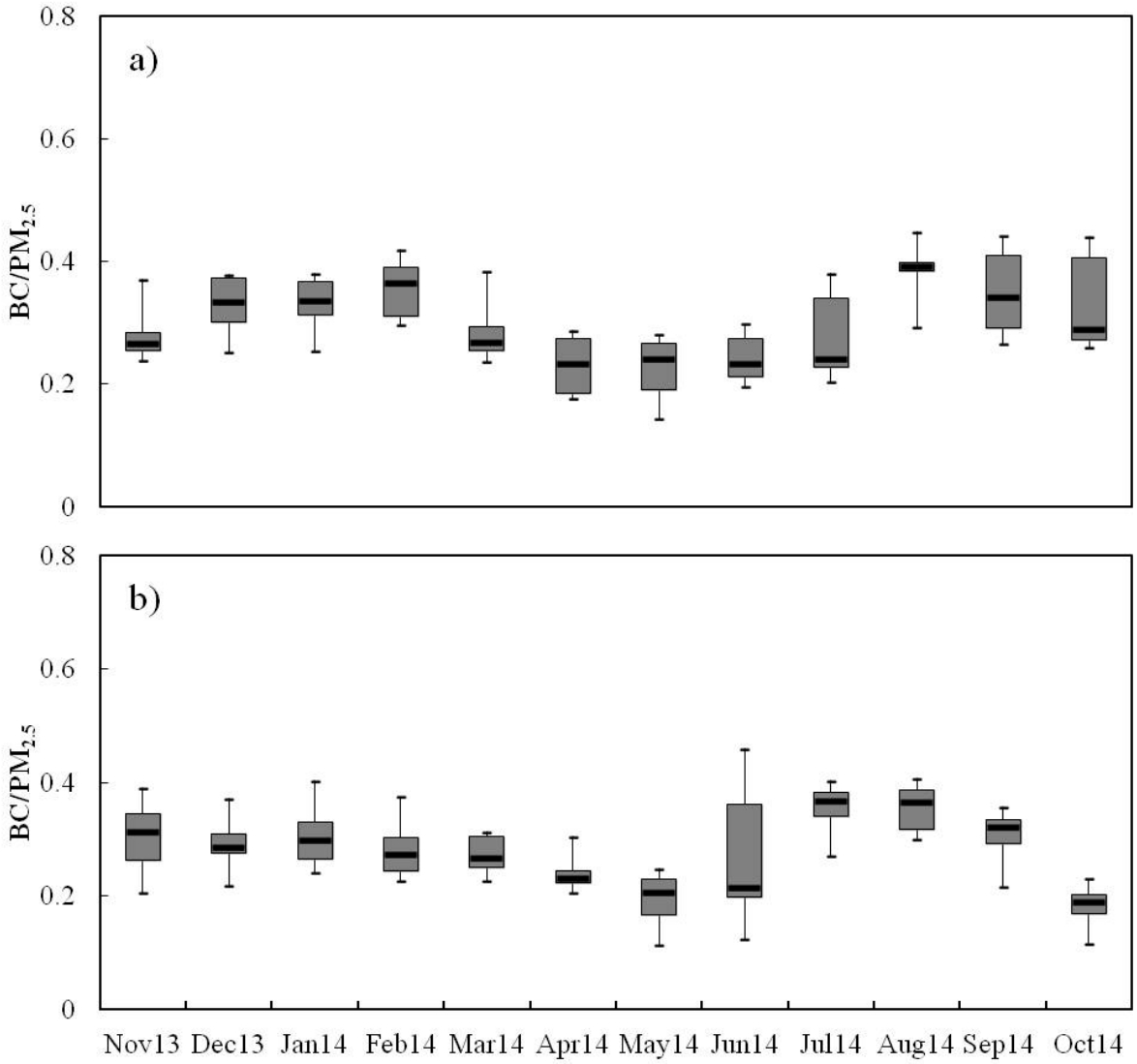

Fig. 4 Monthly BC to $PM_{2.5}$ mass ratio (a) urban site (b) rural site. The box represents 25–75% whereas the whiskers represent the upper 25% and lower 25% of the distributions of the monthly $PM_{2.5}$ concentration. The horizontal line in the box indicates the median of the distribution for the month.

The average of BC concentrations at various locations is presented in Table 1 along with the levels of the current study. The BC levels observed during the current study were in good comparison with those reported for urban sites (e.g. Begum et al., 2012; Chen et al., 2016; Hung et al., 2014). However, the BC values were much higher even at the rural site of Phitsanulok, because of the proximity of traffic emissions when compared to a hilltop rural city, Sinhagad, India (Raju et al., 2011), a rural site of Ballia, India (Tiwari et al., 2016) and a remote rural site in Tibet (Engling et al., 2011).

Table 1 Black carbon (BC) concentrations at different locations

Location	Type	Range of BC ($\mu g\ m^{-3}$)	Reference
Xi'an, China	Urban	2-65	Cao et al., 2009
Bangkok, Thailand	Urban roadside	15-44	Hung et al., 2014b
Sinhagad, India	Rural	0.9-2.2	Raju et al., 2011
Ballia, India	Rural	2.4 - 5.6	Tiwari et al., 2016
Tengchong, Tibet	Remote rural	0.04-1.4	Engling et al., 2011
Dhaka, Bangladesh	Urban	4–48	Begum et al., 2012
Mumbai, India	Urban industrial	1-9.4	Sandeep et al., 2013
Beijing, China	Urban	1.0 - 12. 9	Chen et al., 2016
Phitsanulok, Thailand	Urban	14.5-29	This study
Phitsanulok, Thailand	Rural	6.8-15.4	This study

3.3 Possible long range transport of BC

Trajectory analysis was used to identify the sectors for BC sources for the samples collected at the sites. The atmospheric samples at Phitsanulok sites were affected by air mass trajectories from westerly wind (46 of 120, 38.3%) more than southerly wind (25.8%), easterly wind (27.5%) and inland (8.4%). Frequency of air mass based on trajectory analysis during study period shown in Fig.5. Based on trajectory analysis, it found that most winds during dry season came from the east. This may indicate that the high BC concentration during dry season was dominated by the easterly wind. On the other hand, the main air mass during wet season was associated with westerly winds.

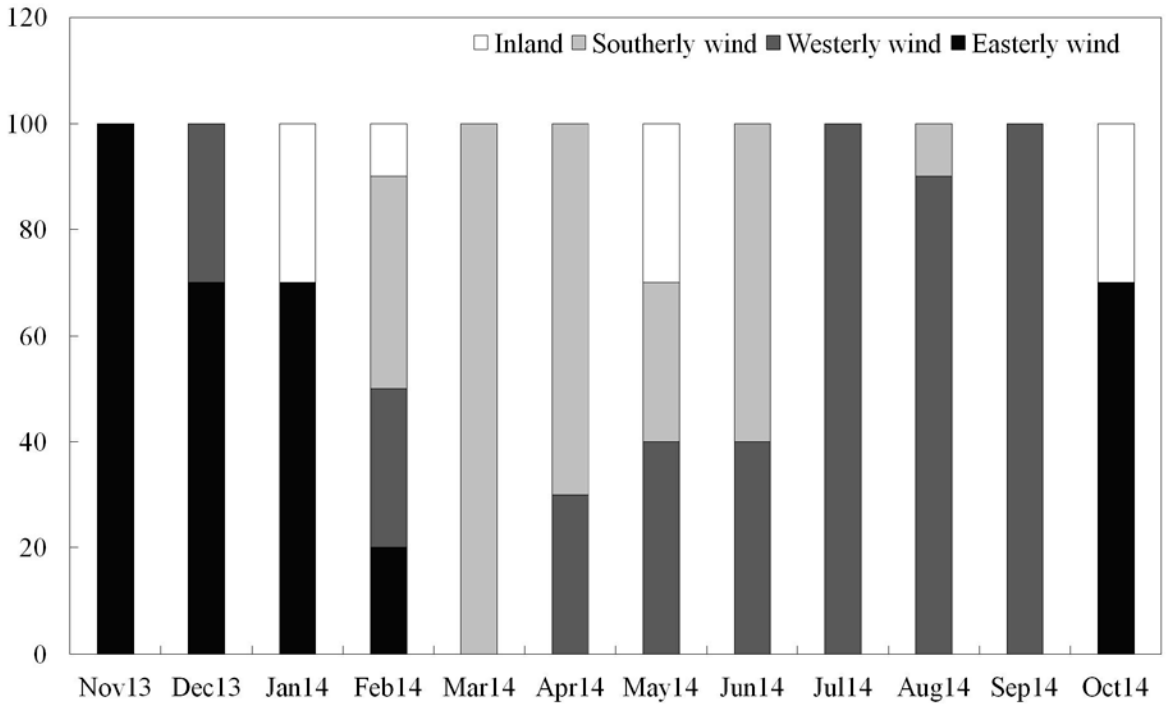

Fig. 5 Frequency of air mass based on trajectory analysis

BC particles have the possibility of migrating long distances in the atmosphere as the lifetime of BC particles is 7–10 days (Babu & Moorthy, 2001). In the current study, high BC levels were observed on few sampling days (19^{th} - 21^{st} February) at both sampling sites. These high concentrations could be either contributed from local sources or from distant sources through long range transport of pollutants.

HYSPLIT model was used to determine the possibility of contribution from long range transport of BC at the sampling sites. To study the contribution of long range transport of BC, the high levels were considered for analysis. There were 3 days (19^{th} - 21^{st} February) during the dry season. Fig. 6 presents the backward trajectories during high BC levels for the above mentioned dates. As shown in Fig. 6, all the 3 day backward trajectories during these days were originated from the northern part of Thailand and Cambodia. In this region of Thailand, high intensity biomass burning has been reported by several researchers (Chuang et al., 2013; Chuang et al., 2016; Phairuang et al. 2007; Sirimongkonlertkul & Phonekeo, 2012) during dry seasons due to open burning, low mixing heights and a stable atmospheric boundary layer. Air trajectories then move towards the southwest which contributes to the high BC concentrations observed at the study sites. However, correlation between BC concentration and the number of hotspot was low at urban and rural sites, with Pearson correlation coefficients of 0.12 ($p < 0.096$, $n = 120$), and of 0.13 ($p < 0.083$, $n = 120$), respectively as shown in Fig. 7. In addition, during dry season the local meteorological conditions such as low mixing height also influences the BC contributed by local sources. It is therefore difficult to distinguish both sources using only BC measurements. By studying both organic carbon and BC fractions and their ratios, it is possible to distinguish different sources contributing to BC levels in Phitsanulok. However, more data is required to confirm this supposition.

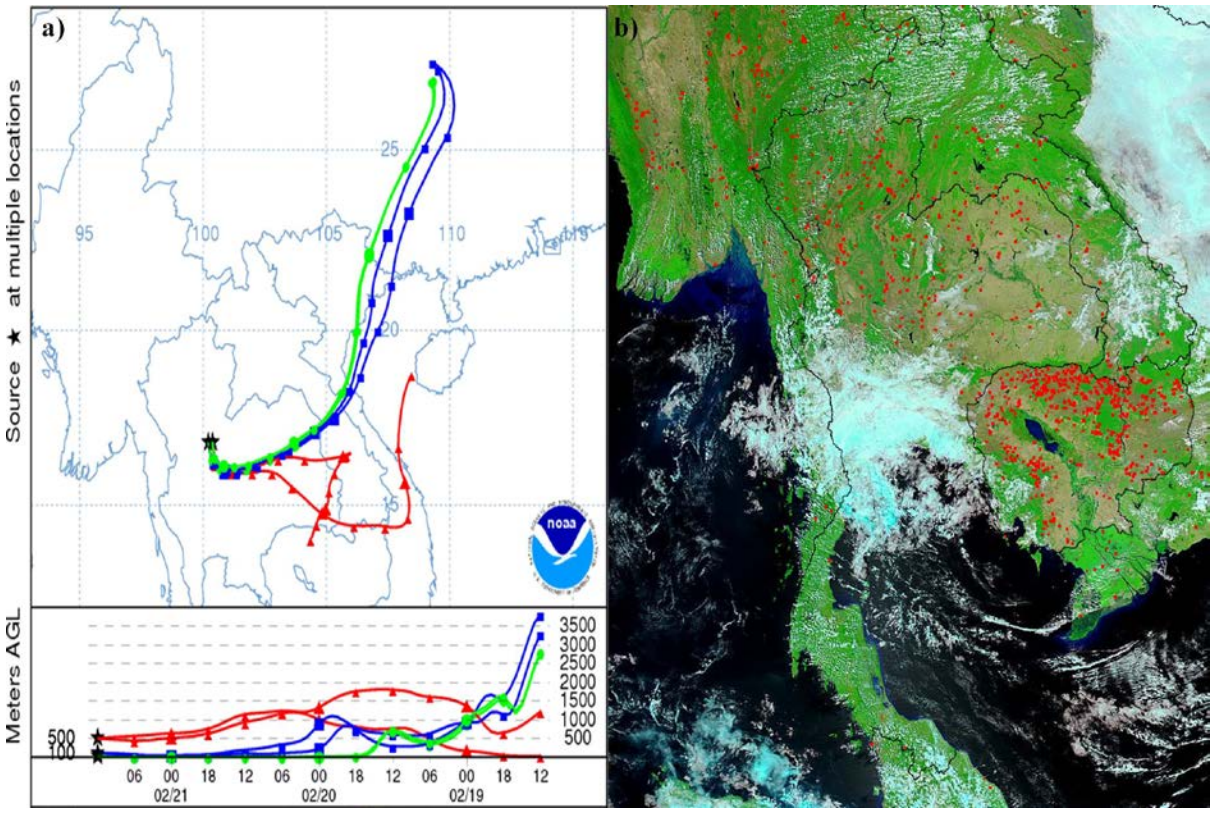

Fig. 6 (a) HYSPLIT backward trajectories for the episodes of high level of BC from 19th to 21st February 2014 (b) MODIS fire distribution.

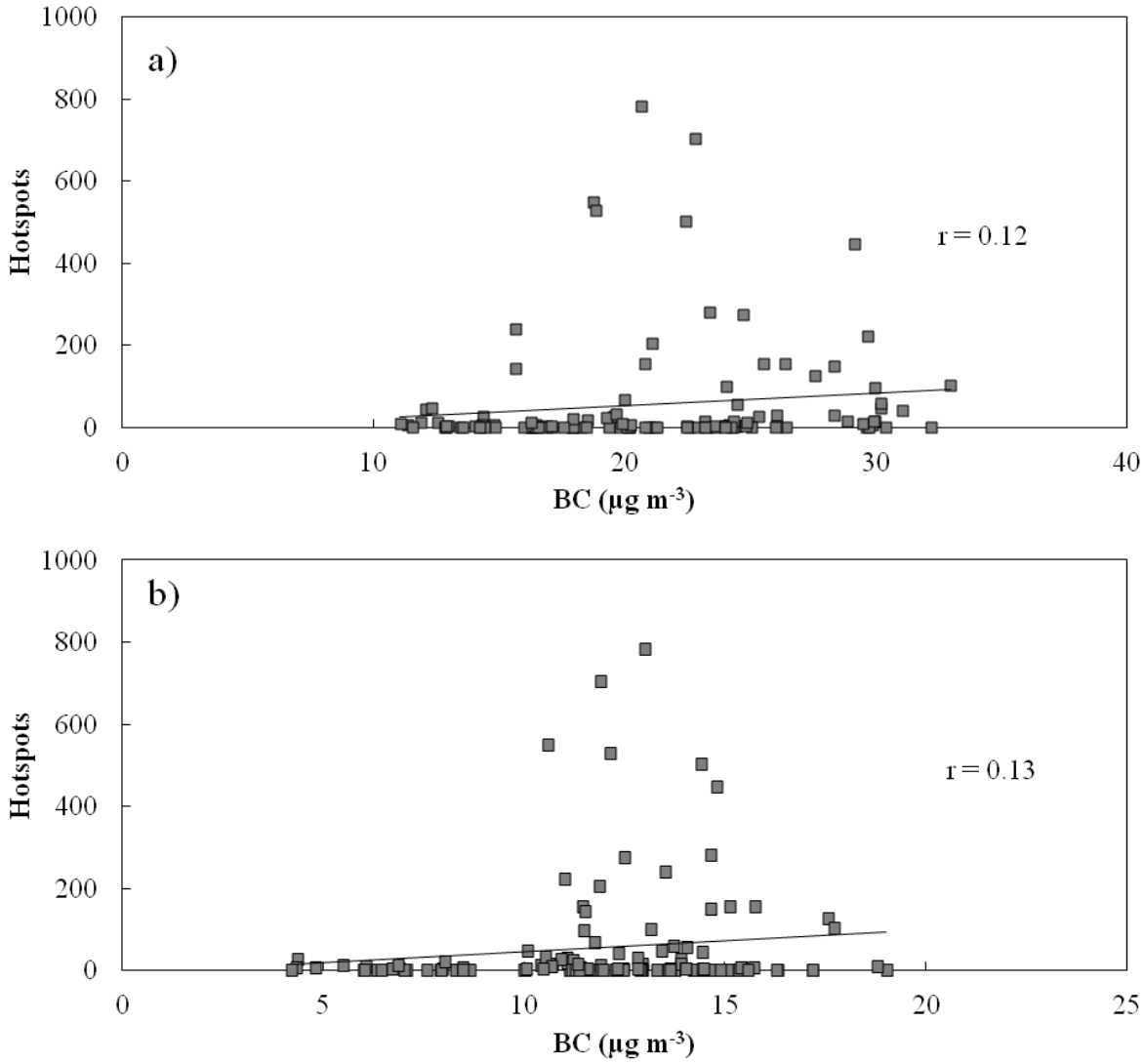

Fig. 7 Scatter plots and Pearson correlation coefficients (r) between BC concentrations and number of hotspot (a) urban site (b) rural site.

CHAPTER 4: CONCLUSIONS AND FURTHER RESEARCH

4.1 conclusions

The concentrations of $PM_{2.5}$ and black carbon (BC) in $PM_{2.5}$ were measured during November 2013 to October 2014 at urban and rural sites of Phitsanulok. $PM_{2.5}$ ranged from 60.7 - 80.3 μg m^{-3} and 36.6 - 48.4 μg m^{-3} for the urban and rural sites, respectively. $PM_{2.5}$ showed trends with high values during dry season (46.8-79.8 μg m^{-3}) and low values during wet season (36.1-61.9 μg m^{-3}). The seasonal average BC concentration ranged from 15.6 - 29.0 μg m^{-3} during dry season compared to 14.5 - 23.8 μg m^{-3} in wet season in an urban site with accounted for 22-38% in $PM_{2.5}$. The BC of a rural site ranged from 11.1 - 15.4 μg m^{-3} and 6.8 - 13.5 μg m^{-3} with accounted for 19-36% in $PM_{2.5}$. The backward trajectory can be indicated the dominant sources of BC at this site are both local and regional. The local sources are traffic and biomass burning. The study also indicates the possible contribution of BC through long range transport from the northern part of Thailand and Cambodia. The findings from this research establish the need to focus on scientifically assessing the local and transboundary air pollution.

4.2 Further research

Research on the potential ability of BC to affect the formation of cloud condensation nuclei (CCN) would be useful. Moreover, the ways in which these compounds interact with metals or/and gases in aqueous aerosol chemistry are not fully understood. Thus, the study of fractions of BC in water droplets and their heterogeneous reactions on atmospheric particles in further work could lead to a better understanding of the BC in atmosphere.

The effects of atmospheric BC on human health should also be studied; its toxic effects on human health, animals and aquatic organisms need to be investigated. Based on research findings, the studies agreed that BC is an indirect indicator should lead to a reduction in the health effects associated with PM. It also recommended that the use of BC as an additional

indicator may be useful in evaluating local action aimed at reducing the population's exposure to combustion PM.

The present level of scientific understanding of atmospheric chemistry of aerosols requires further work. The importance of atmospheric aerosols has encouraged much research intended to study their loading, distribution, and properties for developing understanding of the controlling processes of air pollution, acid deposition, and climate influences of aerosols. However, the current state of explanation based on measurements is inadequate to understand the characterization of aerosol properties. These limitations are still more serious for predictions of future emissions and impacts thus they will provide motivation for theoretical studies for developing the understanding for atmospheric aerosols.

REFERENCES

Ackerman, A.S., Toon, O.B., Stevens, D.E., Heymsfield, A.J., Ramanathan, V., Welton, E.J., 2000. Reduction of tropical cloudiness by soot. Science 288, 1042-1047.

Adams, H.S. Nieuwenhuijsen, M.J. Colvile, R.N. Older, M.J. Kendall, M., 2002. Assessment of road users' elemental carbon personal exposure levels. Atmospheric Environment 36, 5335–5342.

Ahmed, T., Dutkiewicz, V.A., Shareef, A., Tuncel, G., Tuncel, S., Husain, L., 2009. Measurement of black carbon (BC) by an optical method and a thermal-optical method: Intercomparison for four sites. Atmospheric Environment 43, 6305-6311.

Andreae, M.O., 1995. Climatic effects of changing atmospheric aerosol levels, in: World Survey of Climatology, Future Climates of the World, edited by: Henderson-Sellers, A., Elsevier, Amsterdam 16, 341–392,

Andreae, M.O., 1983. Soot carbon and excess fine potassium: Longrange transport of combustion-derived aerosols, Science 220, 1148–1151.

Andreae, M.O., Gelencsér, A., 2006. Black carbon or brown carbon? The nature of light-absorbing carbonaceous aerosols. Atmospheric Chemistry and Physics 6, 3131-3148.

Babu, S.S., Moorthy, K.K., 2001. Anthropogenic impact on aerosol black carbon mass concentration at a tropical coastal station: A case study. Current Science 81, 1208-1214.

Babu, S.S., Moorthy, K.K., 2002. Aerosol black carbon over a tropical coastal station in India. Geophysical Research Letters 29, 11-14.

Badarinath, K.V., Kharol, S.K., Latha, K.M., Chand, T.R., Prasad, V.K., Jyothsna, A.N., Samatha, K., 2007, Multiyear ground‐based and satellite observations of aerosol properties over a tropical urban area in India. Atmospheric Science Letters 8, 7-13.

Badarinath, K.V., Kharol, S.K., Reddy, R.R., Rama Gopal, K. , Narasimhulu, K. , Siva Sankara Reddy, L., Raghavendra Kumar, K., 2009. Black carbon aerosol mass concentration variation in urban and rural environments of India—a case study. Atmospheric Science Letters 10, 29-33.

Begum, B.A., Hossain, A., Nahar, N., Markwitz, A., Hopke, P.K., 2012. Organic and black carbon in $PM_{2.5}$ at an urban site at Dhaka, Bangladesh. Aerosol and Air Quality Research 12, 1062-1072.

Bockhorn, H., 1994. Soot Formation in Combustion: Mechanisms and Models, Berlin & New York, Springer-Verlag.

Bond, T.C., Sun, H.L., 2005. Can reducing black carbon emissions counteract global warming?. Environmental Science & Technology 39, 5921– 5926.

Brimblecombe, P., 1987. The Big Smoke: A History of Air Pollution in London since Medieval Times. Methuen, London.

Cao, J., Lee, S., Ho, K., Fung, K., Chow, J.C., Watson, J.G., 2006. Characterization of roadside fine particulate carbon and its eight fractions in Hong Kong. Aerosol and Air Quality Research 6, 106-122.

Cao, J.J., Zhu, C.S., Chow, J.C., Watson, J.G., Han, Y.-M., Wang, G.H., Shen, Z.X., An, Z.-S., 2009. Black carbon relationships with emissions and meteorology in Xi'an, China. Atmospheric Research 94, 194-202.

Chameides, W.L., Yu, H., Liu, S. C., Bergin, M., Zhou, X., Mearns, L., Wang, G., Kiang, C. S., Saylor, R. D., Luo, C., Huang Y., Steiner, A., Giorgi. F.,1999. Case study of the effects of atmospheric aerosols and regional haze on agriculture: an opportunity to enhance crop yields in China through emission controls? Proceedings of the National Academy of Sciences of the United States of America 96 (24), 13626–13633.

Chen, L.W., Doddridge, B.G., Dickerson, R.R., Chow, J.C., Mueller, P.K., Quinn, J., Butler, W.A., 2001. Seasonal variations in elemental carbon aerosol, carbon monoxide and sulfur dioxide: Implications for sources. Geophysical Research Letters 28, 1711-1714.

Chen, Y., Schleicher, N., Fricker, M., Cen, K., Liu, X.L., Kaminski, U., Yu, Y., Wu, X.F., Norra, S., 2016. Long-term variation of black carbon and $PM_{2.5}$ in Beijing, China with respect to meteorological conditions and governmental measures. Environmental Pollution 212, 269-278.

Chow, J.C., Watson, J.G., Chen, L.W.A., Paredes-Miranda, G., Chang, M.C.O., Trimble, D., Fung, K.K., Zhang, H., Zhen Yu, J., 2005. Refining temperature measures in thermal/optical carbon analysis. Atmospheric Chemistry and Physics 5(4), 2961–2972.

Chow, J.C., Watson, J.G., Doraiswamy, P., Chen, L.W. A., Sodeman, D.A., Lowenthal, D.H., Park, K., Arnott, P., Motallebi, N., 2009 . Aerosol light absorption, black carbon, and elemental carbon at the Fresno Supersite, California. Atmospheric Research 93, 874–887.

Chow, J.C., Watson, J.G., Pritchett, L.C., Pierson, W.R., Frazier, C.A., Purcell, R. G., 1993. The dri thermal/optical reflectance carbon analysis system: description, evaluation and applications in U.S. Air quality studies, Atmospheric Environment. Part A. General Topics *27*(8), 1185-1201.

Chuang, M.T., Chou, C.C.K., Sopajaree, K., Lin, N.H., Wang, J.L., Sheu, G.R., Chang, Y.J., Lee, C.T., 2013. Characterization of aerosol chemical properties from near-source biomass burning in the northern Indochina during 7-SEAS/Dongsha experiment. Atmospheric Environment 78, 72-81.

Chuang, M.T., Lee, C.T., Chou, C.C.K., Engling, G., Chang, S.Y., Chang, S.C., Sheu, G.R., Lin, N.H., Sopajaree, K., Chang, Y.J., Hong, G.J., 2016. Aerosol transport from Chiang Mai, Thailand to Mt. Lulin, Taiwan – Implication of aerosol aging during long-range transport. Atmospheric Environment 137, 101-112.

Chung, S.H., Seinfeld, J.H., 2005. Climate response of direct radiative forcing of anthropogenic black carbon. Journal of Geophysical Research 110(D11102), 25.

Climate and Clean Air Coalition. 2015. Black Carbon Finance Study Group report. http://www.ccaccoalition.org/en/BCFSGreport.

Colbeck, I., Appleby, L., Hardman, E.J., Harrison, R.M.,1990. The optical properties and morphology of cloud-processed carbonaceous smoke, Journal of Aerosol Science 21, 527–538.

Engling, G., Zhang, Y.N., Chan, C.Y., Sang, X.F., Lin, M., Ho, K.F., Li, Y.S., Lin, C.Y., Lee, J.J., 2011. Characterization and sources of aerosol particles over the southeastern Tibetan Plateau during the Southeast Asia biomass-burning season. Tellus B 63, 117–128.

Field, L., Ivanova, D., Bhattacharyya, S.,Mlaker, V., Sholtz, A., Decca, R., et al. 2018. Increasing Arctic sea ice albedousing localized reversible geoengineering. Earth's Future 6, 882–901.

Forbes, M.S., Raison, R.J., Skjemstad, J.O., 2006. Formation, transformation and transport of black carbon (charcoal) in terrestrial and aquatic ecosystem. Science of the Total Environment 370, 190-206.

Fruin, S.A., Winer, A.M., Rodes, C.E., 2004. Black carbon concentrations in California vehicles and estimation of in vehicle diesel exhaust particulate matter exposures. Atmospheric Environment 38, 4123–4133.

Gold, D.R., Litonjua, A.A., Zanobetti, A., Coull, B.A., Schwartz, J., MacCallum, G., Verrier, R.L., Nearing, B.D., Canner, M.J., Suh, H. Stone, P.H., 2005. Air pollution and ST-segment depression in elderly subjects. Environmental Health Perspectives 113 (7), 883-887.

Goldberg, E. D., 1985. Black Carbon in the Environment: Properties and Distribution, New York, J. Wiley & Sons.

Gotschi, T., Oglesby, L., Mathys, P., Monn, C., Manalis, N., Koistinen, K., Jantunen, M., Hanninen, O., Polanska, L., Kunzli, N., 2002. Comparison of black smoke and $PM_{2.5}$ levels in indoor and outdoor environments of four European cities. Environmental Science and Technology 36, 1191–1197.

Grisdale, R.O., 1953. The formation of black carbon, Journal of Applied Physics 24, 1082–1091.

Guo, L.C., Bao, L.J., She, J.W., Zeng, E.Y., 2014. Significance of wet deposition to removal of atmospheric particulate matter and polycyclic aromatic hydrocarbons: A case study in Guangzhou, China. Atmospheric Environment 83, 136-144.

Han, Y.M., Cao, J.J., Chow, C.C., Watson, G., An, Z.S, Jin, Z., Fung, K., Liu, S., 2007. Evaluation of the thermal/optical reflectance method for discrimination between char- and soot-EC. Chemosphere 69, 569–574.

Han Y. M., Cao, J.J., Lee, S.C., Ho, K. F., An Z.S., 2010. Different characteristics of char and soot in the atmosphere and their ratio as an indicator for source identification in Xi'an, China. Atmospheric Chemistry and Physics 10, 595–607.

Hansen, A.D.A., Rosen, H., Novakov, T., 1984. The aethalometer - An instrument for the real-time measurement of optical absorption by aerosol particles. Science of The Total Environment 36, 191-196.

Hansen, J.E., Sato, M., Lacis, A., Ruedy, R., Tegen, I., Matthews, E., 1998. Climate forcings in the industrial era, Proceedings of the National Academy of Sciences 95, 753–758.

Hansen, J., Nazarenko, L., 2004. Soot climate forcing via snow and ice albedos, Proceedings of the National Academy of Sciences 101, 423–428.

Hansen, J., Sato, M., Reudy, R., Lacis, A., Oinas, V., 2000. Global warming in the 21st Century: an alternative scenarios. Proceedings of the National Academy of Sciences 97, 9875–9880.

Hansen, J., Sato, M., Ruedy, R., Nazarenko, L., Lacis, A., Schmidt, G.A., Russell, G., Aleinov, I., Bauer, M., Bauer, S., Bell, N., Cairns, B., Canuto, V., Chandler, M., Cheng, Y., Del Genio, A., Faluvegi, G., Fleming, E., Friend, A., Hall, T., Jackman, C., Kelley, M., Kiang, N., Koch, D., Lean, J., Lerner, J., Lo, K., Menon, S., Miller, R., Minnis, P., Novakov, T., Oinas, V., Perlwitz, J., Perlwitz, J., Rind, D., Romanou, A., Shindell, D., Stone, P., Sun, S., Tausnev, N., Thresher, D., Wielicki, B., Wong, T., Yao, M., Zhang, S., 2005. Efficacy of Climate Forcings, Journal of Geophysical Research 110, D18104.

Haywood, J., Boucher, O., 2000. Estimates of the direct and indirect radiative forcing due to tropospheric aerosols: A review, Reviews of Geophysics 38(4), 513–543.

Heintzenberg, J., 1982. Size-segregated measurements of particulate elemental carbon and aerosol light absorption at remote locations, Atmospheric Environment 16, 2461–2469.

Henneberger, A., Zareba, W., Ibald-Mulli, A., Rückerl, R., Cyrys, J., Couderc, J.P., Mykins, B., Woelke, G., Wichmann, H.E. Peters, A., 2005. Repolarization changes induced by air pollution in ischemic heart disease patients. Environmental Health Perspectives 113(4), 440-446.

Hitzenberger, R., Petzold, A., Bauer, H., Ctyroky, P., Pouresmaeil, P., Laskus, L., Puxbaum H., 2006. Intercomparison of thermal and optical measurement methods for elemental carbon and black carbon at an urban location. Environmental Science & Technology 40, 6377–6383.

Hitzenberger, R., Fohler-Norek, C., Dusek, U., Galambos, Z., Sidla, S., 1996. Comparison of recent (1994/1996) black carbon (BC) data with those obtained in 1985 and 1986 in the urban area of Vienna, Austria. Journal of Aerosol Science 27, Supplement 1, S51-S52.

Hoek, G., Brunekreef, B., Goldbohm, S., Fischer, P., van den Brandt, P., 2002. Association between mortality and indicators of traffic-related air pollution in the Netherlands: a cohort study. The Lancet 360, 1203–1209.

Hung, N.T.Q., Lee, S.-B., Hang, N.T., Kongpran, J., Kim Oanh, N.T., Shim, S.-G., Bae, G.-N., 2014. Characterization of black carbon at roadside sites and along vehicle roadways in the Bangkok Metropolitan Region. Atmospheric Environment 92, 231-239.

Husain, L., Dutkiewicz, V.A., Khan, A.J., Ghauri, B.M., 2007. Characterization of carbonaceous aerosols in urban air. Atmospheric Environment 41, 6872–6883.

Invernizzi, G., Ruprecht, A., Mazza, R., De Marco, C., Mo**Č**nik, G. Sioutas, C. Westerdahl, D., 2011. Measurement of black carbon concentration as an indicator of air quality benefits of traffic restriction policies within the ecopass zone in Milan, Italy, Atmospheric Environment 45 (21), 3522-3527.

IPCC, 2007. Climate change 2007: The physical science basis summary for policymakers. Contribution of working group I to the fourth assessment report of the Intergovernmental Panel on Climate Change. World Meteorological Organization, Geneva, Switzerland.

ISO. 1993. ISO standard 9835:1993 (E). Ambient air – determination of a black smoke index. Geneva, International Organization for Standardization.

Jacobson, M.Z., 2004. Climate response of fossil fuel and biofuel soot, accounting for soot's feed back to snow and sea ice albedo and emissivity. Journal of Geophysical Research 109, (D21201), 15.

Jacobson, M. Z., 2002. Control of fossil-fuel particulate black carbon and organic matter, possibly the most effective method of slowing global warming, Journal of Geophysical Research 107, 4410.

Jacobson, M.Z., 2001. Strong radiative heating due to the mixing state of black carbon in atmospheric aerosols. Nature 409, 695-697.

Janssen, N.A., Hoek, G., Simic-Lawson, M., Fischer, P., van Bree, L., ten Brink, H., Keuken, M., Atkinson, R.W., Anderson, H.R., Brunekreef, B., Cassee, F.R., 2011. Black carbon as an additional indicator of the adverse health of airborne particles compared to PM_{10} and $PM_{2.5}$. Environmental Health Perspectives 119, 1691–1699.

Jones, G.S., Jones, A., Roberts, D.L., Stott, P.A., Williams, K.D., 2005. Sensitivity of global scale climate change attribution results to inclusion of fossil fuel black carbon aerosol. Geophysical Research letter 32, (L14701), 4.

Kanaya, Y., Taketani, F., Komazaki, Y., Liu, X., Kondo, Y., Sahu, L.K., Irie, H., Takashima, H., 2013. Mass concentrations of black carbon measured by four instruments in the middle of Central East China in June 2006. Atmospheric Chemistry and Physics 8, 7637–7649.

Kanokkanjana, K., Penwadee, C., Savitri,G., 2011. Black Carbon Emission from Paddy Field Open Burning in Thailand. 2nd International Conference on Environmental Science and Technology. IPCBEE 6, 88-92.

Katsouyanni, K., Touloumi, G., Samoli, E., Gryparis, A., Le Tertre, A., Monopolis, Y., Rossi, G., Zmirou, D., Ballester, F., Boumghar, A., Anderson, H.R., Wojtyniak, B, Paldy, A., Braunstein, R., Pekkanen, J., Schindler, C., Schwartz, J., 2001. Confounding and effect modification in the short-term effects of ambient particles on total mortality: results from 29 European cities within APHEA2 project. Epidemiology 12, 521–531.

Kumar, K.R., Narasimhulu, K., Balakrishnaiah, G., Reddy, B.S.K., Gopal, K.R. Reddy, R.R., Satheesh, S.K., Moorthy, K.K., Babu, S.S., 2011. Characterization of aerosol black carbon over a tropical semi-arid region of Anantapur, India. Atmospheric Research 100(1), 12-27.

Lanki, T., Ahokas, A., Alm, S., Janssen, N.A., Hoek, G., De Hartog, J.J., Brunekreef, B., Pekkanen, J., 2007. Determinants of personal and indoor $PM_{2.5}$ and absorbance among elderly subjects with coronary heart disease. Journal of Exposure Science and Environmental Epidemiology 17, 124–133.

Larson, T., Gould, T., Simpson, C., Liu, L.J., Claiborn, C., Lewtas, J., 2004. Source apportionment of indoor, outdoor, and personal $PM_{2.5}$ in Seattle, Washington, using positive matrix factorization. Journal Air & Waste Management Association 54, 1175–1187.

Levin, Z. and Lindberg, J. D., 1979. Size distributions, chemical composition, and optical properties of urban and desert aerosols in Israel, Journal of Geophysical Research 84, 6941–6950.

Lin, W., Huang, W., Zhu, T., Hu, M., Brunekreef, B., Zhang, Y., Liu, X., Cheng, H., Gehring, U., Li, C. and Tang X., 2011. Acute respiratory inflammation in children and black carbon in ambient air before and during the 2008 Beijing Olympics. Environmental Health Perspectives 119, 1507–1512.

Liousse, C., Cachier, H., Jennings, S.G., 1993. Optical and thermal measurements of black carbon aerosol content in different environments: Variation of the specific attenuation cross-section, sigma (σ). Atmospheric Environment. Part A. General Topics 27, 1203-1211.

Lunden, M.M., Kirchstetter, T.W., Thatcher, T.L., Hering, S.V., Brown, N.J., 2008. Factors affecting the indoor concentrations of carbonaceous aerosols of outdoor origin. Atmospheric Environment 42, 5660–5671.

Mader, B.T., Flagan, R.C., Seinfeld, J.H., 2002.Airborne measurements of atmospheric carbonaceous aerosols during ACE-Asia. Journal of Geophysical Research 107(D23), 4704.

Martins, J. V., Hobbs, P. V., Weiss, R. E., Artaxo, P., 1998. Sphericity and morphology of smoke particles from biomass burning in Brazil, Journal of Geophysical Research 103, 051–057,

Masiello, C.A., 2004. New directions in black carbon organic geochemistry. Marine Chemistry 92, 201-213.

Mayol-Bracero, O.L., Gabriel, R., Andreae, M.O., Kirchstetter, T.W., Novakov, T., Ogren, J., Sheridan, P., Streets, D.G., 2002. Carbonaceous aerosols over the Indian Ocean during the Indian Ocean Experiment (INDOEX): Chemical characterization, optical properties, and probable sources. Journal of Geophysical Research: Atmospheres 107, INX2 29-21-INX22 29-21.

McMeeking, G. R., Hamburger, T., Liu, D., Flynn, M., Morgan, W. T., Northway, M., Highwood, E. J., Krejci, R., Allan, J. D., Minikin, A., Coe, H., 2010. Black carbon measurements in the boundary layer over western and northern Europe, Atmospheric Chemistry and Physics 10, 9393-9414.

Medalia, A. I. Rivin, D., 1982. Particulate carbon and other components of soot and carbon black, Carbon 20, 481–492.

Menon, S., Hanse, J., Nazerenko, L., Luo, Y.F., 2002. Climate effects of black carbon aerosols in China and India. Science 297, 2250–2253.

Müller, T., Henzing, J. S., de Leeuw, G., Wiedensohler, A., Alastuey, A., Angelov, H., Bizjak, M., Collaud Coen, M., Engström, J. E., Gruening, C., Hillamo, R., Hoffer, A., Imre, K., Ivanow, P., Jennings, G., Sun, J. Y., Kalivitis, N., Karlsson, H., Komppula, M., Laj, P., Li, S.-M., Lunder, C., Marinoni, A., Martins dos Santos, S., Moerman, M., Nowak, A., Ogren, J. A., Petzold, A., Pichon, J. M., Rodriquez, S., Sharma, S., Sheridan, P. J., Teinilä, K., Tuch, T., Viana, M., Virkkula, A., Weingartner, E., Wilhelm, R., and Wang, Y. Q., 2011. Characterization and intercomparison of aerosol absorption photometers: result of two intercomparison workshops. Atmospheric Measurements Techniques 4, 245–268.

Oberlin, A., 1989. High-resolution TEM studies of carbonization and graphitization, in: Chemistry and Physics of Carbon, edited by: Thrower, P. A., M. Dekker, New York.

OECD. 1964. Methods of measuring air pollution. Report of the working party on methods of measuring air pollution and survey techniques. Paris, Organisation for Economic Co-operation and Development.

Onischuk, A. A., di Stasio, S., Karasev, V. V., Baklanov, A. M., Makhov, G. A., Vlasenko, A. L., Sadykova, A. R., Shipovalov, A. V., and Panfilov, V. N., 2003. Evolution of structure and charge of soot aggregates during and after formation in a propane/air diffusion flame, Journal of Aerosol Science 34, 383-403.

Petzold, A., Kopp, C., Niessner, R., 1997. The dependence of the specific attenuation cross-section on black carbon mass fraction and particle size. Atmospheric Environment 31, 661-672.

Phairuang, W., Hata, M., Furuuchi, M., 2017. Influence of agricultural activities, forest fires and agro-industries on air quality in Thailand. Journal of Environmental Sciences 52, 85-97.

Puustinen, A., Hämeri, K., Pekkanen, J., Kulmala, M., de Hartog, J., Meliefste, K., ten Brink, H., Kos, G., Katsouyanni, K., Karakatsani, A., Kotronarou, A., Kavouras, I., Meddings, C., Thomas, S., Harrison, R., Ayres, J.G., van der Zee, S., Hoek, G., 2007. Spatial variation of particle number and mass over four European cities. Atmospheric Environment 41, 6622-6636.

Qian, Y., Flanner, M. G., Leung, L. R., Wang, W., 2011. Sensitivity studies on the impacts of Tibetan Plateau snowpack pollution on the Asian Hydrological cycle and Monsoon Climate. Atmospheric Chemistry and Physics, 11, 1929-1948.

Quincey, P., 2007. A relationship between Black Smoke Index and Black Carbon concentration, Atmospheric Environment 41(36), 7964-7968.

Raaschou-Nielsen, O., Sørensen, M., Hertel, O., Chawes, B.L.K., Vissing, N., Bønnelykke, K., Bisgaard, H., 2011. Predictors of indoor fine particulate matter in infants' bedrooms in Denmark. Environmental Research 111, 87-93.

Raju, M.P., Safai, P.D., Rao, P.S.P., Devara, P.C.S., Budhavant, K.B., 2011. Seasonal characteristics of black carbon aerosols over a high altitude station in Southwest India. Atmospheric Research 100, 103-110.

Ramanathan, V. and Y. Feng., 2009. Air pollution, greenhouse gases and climate change: Global and regional perspectives. Atmospheric Environment 43(1), 37-50.

Ramanathan, V., Carmichael G., 2008. Global and regional climate changes due to black carbon. Nature Geoscience 1, 221-227.

Ramanathan, V., Chung, C., Kim, D., Bettge, T., Buja, L., Kiehl, J. T., Washington, W. M., Fu, Q., Sikka, D. R., and Wild, M., 2005. Atmospheric brown clouds: Impacts on South Asian climate and hydrological cycle Proceedings of the National Academy of Sciences 102 (15), 5326-5333.

Ramanathan, V., Crutzen, P.J., 2003. New directions: atmospheric brown clouds. Atmospheric Environment 37, 4033–4035.

Reddy, M.S., Venkataraman, C., 1999. Direct radiative forcing from anthropogenic carbonaceous aerosols over India. Current Science 76, 1005-1011.

Reisinger, P., Wonaschütz, A., Hitzenberger, R., Petzold, A., Bauer, H., Jankowski, N., Puxbaum, H., Chi, X., Maenhaut, W., 2008. Intercomparison of Measurement Techniques for Black or Elemental Carbon Under Urban Background Conditions in Wintertime: Influence of Biomass Combustion. Environmental Science & Technology 42, 884-889.

Ruellan, S., Cachier, H., 2001. Characterisation of fresh particulate vehicular exhausts near a Paris high flow road. Atmospheric Environment 35, 453-468.

Ruellan, S., Cachier, H., Gaudichet, A., Masclet, P., Lacaux, J.P., 1999. Airborne aerosols over central Africa during the experiment for regional sources and sinks of oxidants (EXPRESSO), Journal of Geophysical Research: Atmospheres 104, 673–690.

Salako, G. O., Hopke, P. K., Cohen, D. D., Begum, B. A., Biswas, S. K., Pandit, G. G., Bunprapob, S., 2012. Exploring the Variation between EC and BC in a Variety of Locations. Aerosol and Air Quality Research 12, 1-7.

Sarnat, S.E., Coull, B.A., Ruiz, P.A., Koutrakis, P., Suh, H.H., 2006. The influences of ambient particle composition and size on particle infiltration in Los Angeles, CA, residences. Journal Air & Waste Management Association 56, 186–196.

Schaap, M., Denier van der Gon, H.A.C., 2007. On the variability of Black Smoke and carbonaceous aerosols in the Netherlands. Atmospheric Environment 41, 5908-5920.

Schuster, G.L., Dubovik, O., Holben, B.N., Clothiaux, E.E., 2005. Inferring black carbon content and specific absorption from Aerosol Robotic Network (AERONET) aerosol retrievals. Journal of Geophysical Research: Atmospheres 110, D10S17.

Schwarz, J. P., H. Stark, J. R. Spackman, T. B. Ryerson, J. Peischl, W. H. Swartz, R. S. Gao, L. A. Watts, and D. W. Fahey., 2009. Heating rates and surface dimming due to black carbon aerosol absorption associated with a major U.S. city, Geophysical Research letter 36(15), L15807.

Shindell, D., Faluvegi, G., 2009. Climate response to regional radiative forcing during the twentieth century. Nature Geoscience 2, 294-300.

Singh, S.P., Bassignana-Khadka, I., Karky, B.S., Sharma, E., 2011. Climate change in the Hindu Kush-Himalayas: The state of current knowledge. Kathmandu: ICIMOD. http://lib.icimod.org.

Sirimongkonlertkul, N., Phonekeo, V., 2012. Remote sensing and GIS application analysis of active fire, aerosol optical thickness and estimated PM_{10} in the north of Thailand and Chiang Rai province. APCBEE Procedia 1, 304-308.

Smith, K. R., M. Jerrett, H. R. Anderson, R. T. Burnett, V. Stone, R. Derwent, R. W. Atkinson, A. Cohen, S. B. Shonkoff, D. Krewski, C. A. Pope Iii, M. J. Thun, and G. Thurston., 2009. Public health benefits of strategies to reduce greenhouse-gas emissions: health implications of short-lived greenhouse pollutants. The Lancet 374(9707), 2091-2103.

Stein, A., Draxler, R., Rolph, G., Stunder, B., Cohen, M., Ngan, F., 2015. NOAA's HYSPLIT atmospheric transport and dispersion modeling system. Bulletin of the American Meteorological Society 96, 2059-2077.

Tiwari, S., Dumka, U. C., Hopke, P. K., Tunved, P., Srivastava, A. K., Bisht, D. S., & Chakrabarty, R. K., 2016. Atmospheric heating due to black carbon aerosol during the summer monsoon period over Ballia: A rural environment over Indo-Gangetic Plain. Atmospheric Research 178–179, 393-400.

TMD, 2013. Climate of Thailand Thai Meteorological Department. Ministry of Information and Communication Technology, http://www.tmd.go.th.

Vallius, M., Janssen, N.A.H., Heinrich, J., Hoek, G., Ruuskanen, J., Cyrys, J., Van Grieken, R., de Hartog, J.J., Kreyling, W.G., Pekkanen, J., 2005. Sources and elemental composition of ambient $PM_{2.5}$ in three European cities. Science of The Total Environment 337, 147-162.

Wang, M., Xu, B., Wang, N., Cao, J., Tie, X., Wang, H., Zhu, C., Yang, W., 2016. Two distinct patterns of seasonal variation of airborne black carbon over Tibetan Plateau. Science of The Total Environment 573, 1041-1052.

Wang, X., Westerdahl, D., Chen, L.C., Wu, Y., Hao, J., Pan, X., Guo, X., Zhang, K.M., 2009. Evaluating the air quality impacts of the 2008 Beijing Olympic Games: On-road emission factors and black carbon profiles. Atmospheric Environment 43, 4535-4543.

Weingartner, E., Burtscher, H., and Baltensperger, U., 1997.Hygroscopic properties of carbon and diesel soot particles, Atmospheric Environment 31, 2311–2327.

Wentzel, M., Gorzawski, H., Naumann, K. H., Saathoff, H., and Weinbruch, S., 2003. Transmission electron microscopical and aerosol dynamical characterization of soot aerosols, Journal of Aerosol Science 34, 1347–1370.

White, A. H. and Germer, L. H., 1941. The structure of black carbon, Journal of Chemical Physics 9, 492–502.

WHO. 1979. Sulfur oxides and suspended particulate matter. Geneva, World Health Organization (Environmental Health Criteria, No. 8).

Zeger, S.L., Thomas, D., Dominici, F., Samet, J.M., Schwartz, J., Dockery, D., Cohen, A., 2000. Exposure measurement error in time-series studies of air pollution: concepts and consequences. Environmental Health Perspectives 108, 419–426.

Zhao, S., J. Ming, C. Xiao, W. Sun, and X. Qin., 2012. A preliminary study on measurements of black carbon in the atmosphere of northwest Qilian Shan, Journal of Environmental Sciences 24(1), 152-159.

Zhu, Y., Hinds, W. C., Kim, S., Shen, S., Sioutas, C., 2002. Study of ultrafine particles near a major highway with heavy-duty diesel traffic. Atmospheric Environment 36, 4323-4335.

Zuurbier, M., Hoek, G., Oldenwening, M., Lenters, V., Meliefste, K., van den Hazel, P., Brunekreef, B., 2010. Commuters' exposure to particulate air pollution is affected by mode of transport, fuel type, and route. Environmental Health Perspectives 118, 783–789.

Appendix A

Examples of trajectory analysis during dry season

(December 2013 – February 2014)

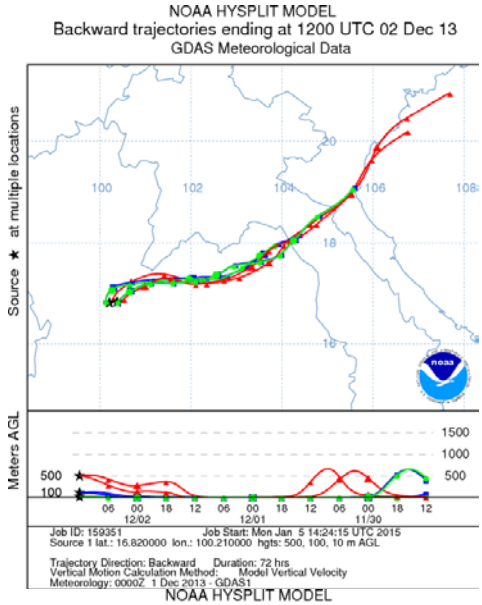
NOAA HYSPLIT MODEL
Backward trajectories ending at 1200 UTC 02 Dec 13
GDAS Meteorological Data
Source ★ at multiple locations
Meters AGL
Job ID: 159351 Job Start: Mon Jan 5 14:24:15 UTC 2015
Source 1 lat.: 16.820000 lon.: 100.210000 hgts: 500, 100, 10 m AGL
Trajectory Direction: Backward Duration: 72 hrs
Vertical Motion Calculation Method: Model Vertical Velocity
Meteorology: 0000Z 1 Dec 2013 - GDAS1

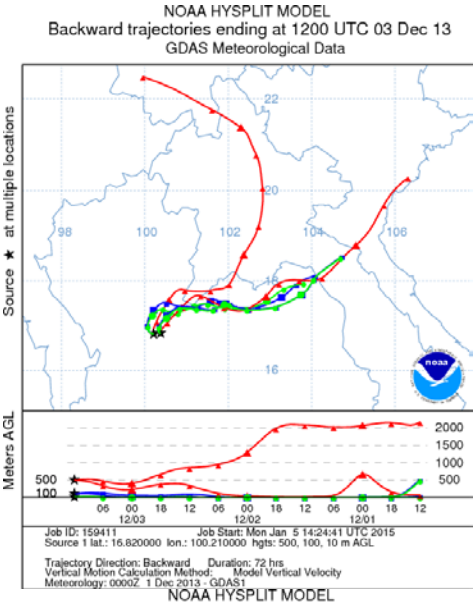
NOAA HYSPLIT MODEL
Backward trajectories ending at 1200 UTC 03 Dec 13
GDAS Meteorological Data
Source ★ at multiple locations
Meters AGL
Job ID: 159411 Job Start: Mon Jan 5 14:24:41 UTC 2015
Source 1 lat.: 16.820000 lon.: 100.210000 hgts: 500, 100, 10 m AGL
Trajectory Direction: Backward Duration: 72 hrs
Vertical Motion Calculation Method: Model Vertical Velocity
Meteorology: 0000Z 1 Dec 2013 - GDAS1

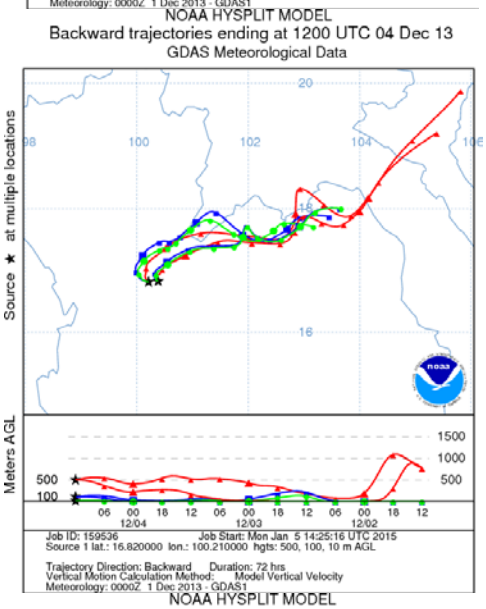
NOAA HYSPLIT MODEL
Backward trajectories ending at 1200 UTC 04 Dec 13
GDAS Meteorological Data
Source ★ at multiple locations
Meters AGL
Job ID: 159536 Job Start: Mon Jan 5 14:25:16 UTC 2015
Source 1 lat.: 16.820000 lon.: 100.210000 hgts: 500, 100, 10 m AGL
Trajectory Direction: Backward Duration: 72 hrs
Vertical Motion Calculation Method: Model Vertical Velocity
Meteorology: 0000Z 1 Dec 2013 - GDAS1

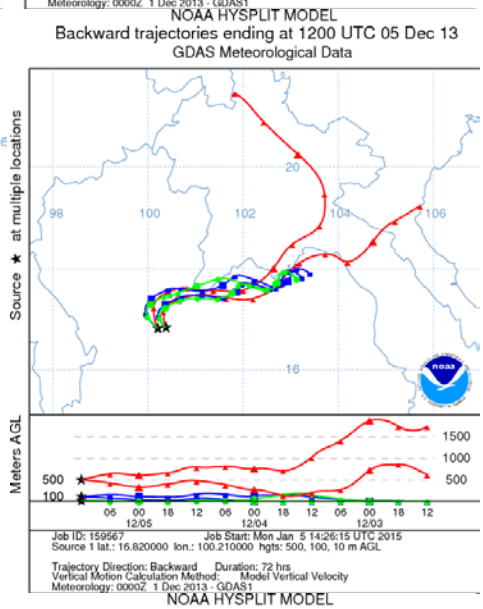
NOAA HYSPLIT MODEL
Backward trajectories ending at 1200 UTC 05 Dec 13
GDAS Meteorological Data
Source ★ at multiple locations
Meters AGL
Job ID: 159567 Job Start: Mon Jan 5 14:26:15 UTC 2015
Source 1 lat.: 16.820000 lon.: 100.210000 hgts: 500, 100, 10 m AGL
Trajectory Direction: Backward Duration: 72 hrs
Vertical Motion Calculation Method: Model Vertical Velocity
Meteorology: 0000Z 1 Dec 2013 - GDAS1

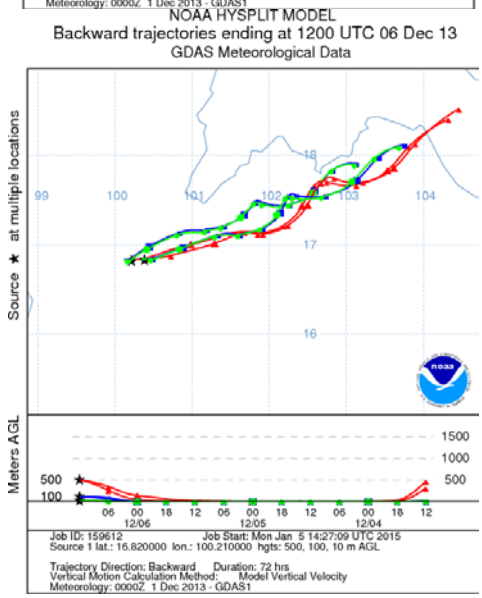
NOAA HYSPLIT MODEL
Backward trajectories ending at 1200 UTC 06 Dec 13
GDAS Meteorological Data
Source ★ at multiple locations
Meters AGL
Job ID: 159612 Job Start: Mon Jan 5 14:27:09 UTC 2015
Source 1 lat.: 16.820000 lon.: 100.210000 hgts: 500, 100, 10 m AGL
Trajectory Direction: Backward Duration: 72 hrs
Vertical Motion Calculation Method: Model Vertical Velocity
Meteorology: 0000Z 1 Dec 2013 - GDAS1

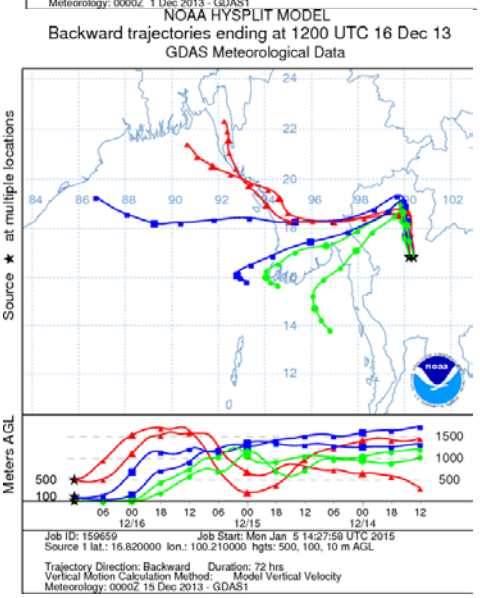
NOAA HYSPLIT MODEL
Backward trajectories ending at 1200 UTC 16 Dec 13
GDAS Meteorological Data
Source ★ at multiple locations
Meters AGL
Job ID: 159659 Job Start: Mon Jan 5 14:27:58 UTC 2015
Source 1 lat.: 16.820000 lon.: 100.210000 hgts: 500, 100, 10 m AGL
Trajectory Direction: Backward Duration: 72 hrs
Vertical Motion Calculation Method: Model Vertical Velocity
Meteorology: 0000Z 15 Dec 2013 - GDAS1

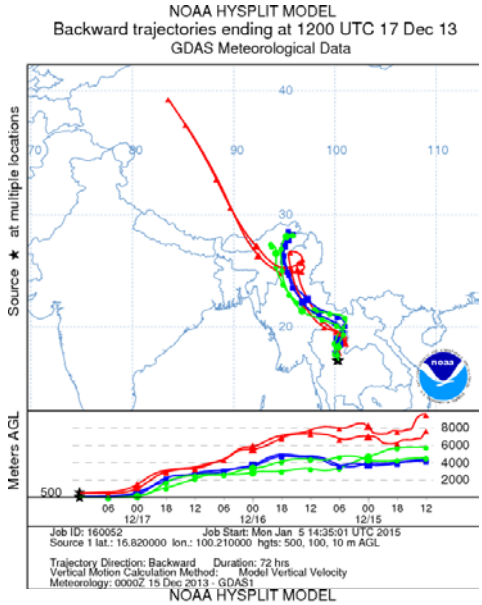
NOAA HYSPLIT MODEL
Backward trajectories ending at 1200 UTC 17 Dec 13
GDAS Meteorological Data
Source ★ at multiple locations
Meters AGL
Job ID: 160052 Job Start: Mon Jan 5 14:35:01 UTC 2015
Source 1 lat.: 16.820000 lon.: 100.210000 hgts: 500, 100, 10 m AGL
Trajectory Direction: Backward Duration: 72 hrs
Vertical Motion Calculation Method: Model Vertical Velocity
Meteorology: 0000Z 15 Dec 2013 - GDAS1

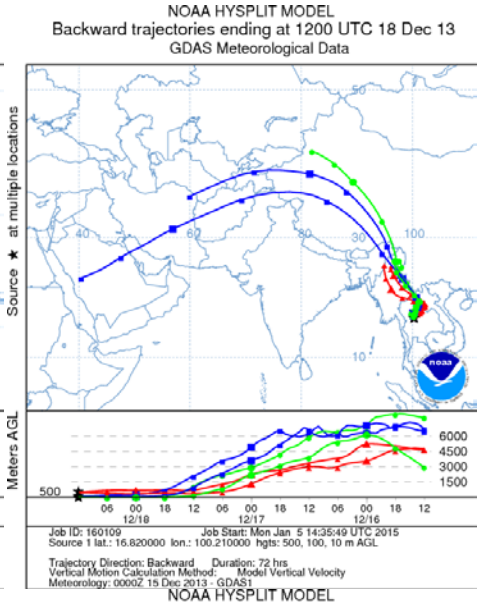
NOAA HYSPLIT MODEL
Backward trajectories ending at 1200 UTC 18 Dec 13
GDAS Meteorological Data
Source ★ at multiple locations
Meters AGL
Job ID: 160109 Job Start: Mon Jan 5 14:35:49 UTC 2015
Source 1 lat.: 16.820000 lon.: 100.210000 hgts: 500, 100, 10 m AGL
Trajectory Direction: Backward Duration: 72 hrs
Vertical Motion Calculation Method: Model Vertical Velocity
Meteorology: 0000Z 15 Dec 2013 - GDAS1

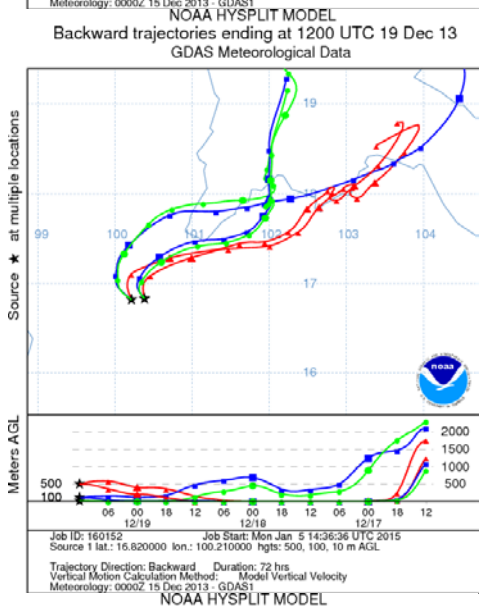
NOAA HYSPLIT MODEL
Backward trajectories ending at 1200 UTC 19 Dec 13
GDAS Meteorological Data
Source ★ at multiple locations
Meters AGL
Job ID: 160152 Job Start: Mon Jan 5 14:36:36 UTC 2015
Source 1 lat.: 16.820000 lon.: 100.210000 hgts: 500, 100, 10 m AGL
Trajectory Direction: Backward Duration: 72 hrs
Vertical Motion Calculation Method: Model Vertical Velocity
Meteorology: 0000Z 15 Dec 2013 - GDAS1

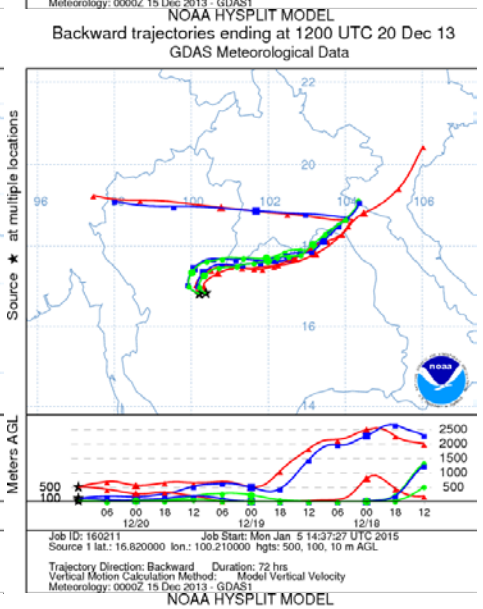
NOAA HYSPLIT MODEL
Backward trajectories ending at 1200 UTC 20 Dec 13
GDAS Meteorological Data
Source ★ at multiple locations
Meters AGL
Job ID: 160211 Job Start: Mon Jan 5 14:37:27 UTC 2015
Source 1 lat.: 16.820000 lon.: 100.210000 hgts: 500, 100, 10 m AGL
Trajectory Direction: Backward Duration: 72 hrs
Vertical Motion Calculation Method: Model Vertical Velocity
Meteorology: 0000Z 15 Dec 2013 - GDAS1

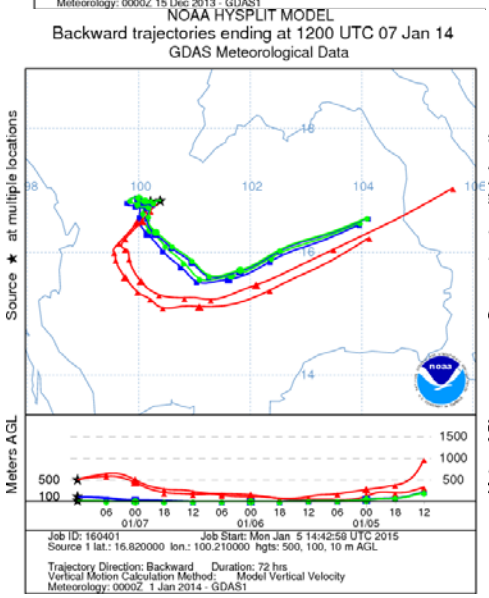
NOAA HYSPLIT MODEL
Backward trajectories ending at 1200 UTC 07 Jan 14
GDAS Meteorological Data
Source ★ at multiple locations
Meters AGL
Job ID: 160401 Job Start: Mon Jan 5 14:42:58 UTC 2015
Source 1 lat.: 16.820000 lon.: 100.210000 hgts: 500, 100, 10 m AGL
Trajectory Direction: Backward Duration: 72 hrs
Vertical Motion Calculation Method: Model Vertical Velocity
Meteorology: 0000Z 1 Jan 2014 - GDAS1

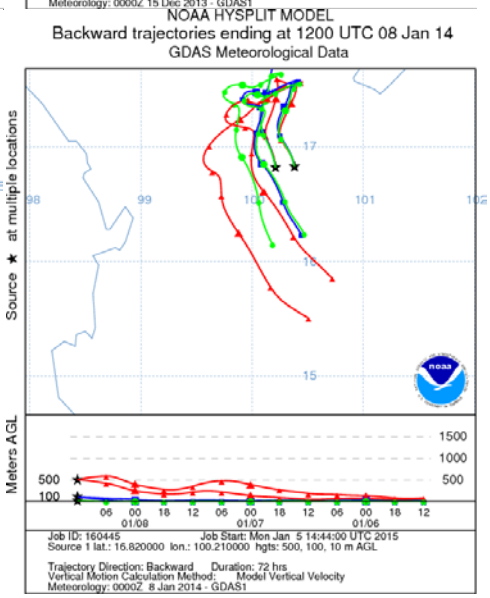
NOAA HYSPLIT MODEL
Backward trajectories ending at 1200 UTC 08 Jan 14
GDAS Meteorological Data
Source ★ at multiple locations
Meters AGL
Job ID: 160445 Job Start: Mon Jan 5 14:44:00 UTC 2015
Source 1 lat.: 16.820000 lon.: 100.210000 hgts: 500, 100, 10 m AGL
Trajectory Direction: Backward Duration: 72 hrs
Vertical Motion Calculation Method: Model Vertical Velocity
Meteorology: 0000Z 8 Jan 2014 - GDAS1

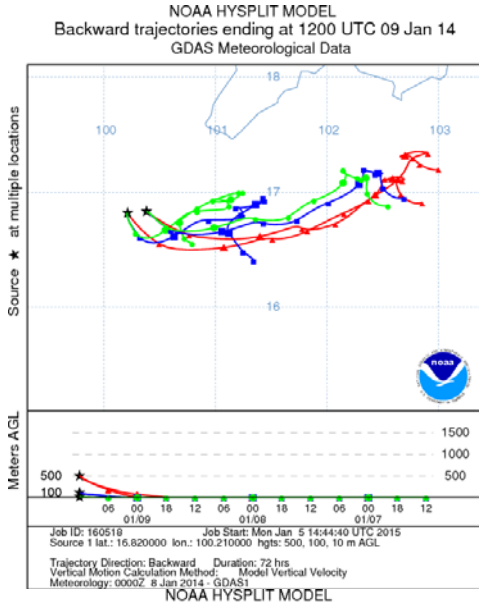
NOAA HYSPLIT MODEL
Backward trajectories ending at 1200 UTC 09 Jan 14
GDAS Meteorological Data
Source ★ at multiple locations
Meters AGL
Job ID: 160518 Job Start: Mon Jan 5 14:44:40 UTC 2015
Source 1 lat.: 16.820000 lon.: 100.210000 hgts: 500, 100, 10 m AGL
Trajectory Direction: Backward Duration: 72 hrs
Vertical Motion Calculation Method: Model Vertical Velocity
Meteorology: 0000Z 8 Jan 2014 - GDAS1

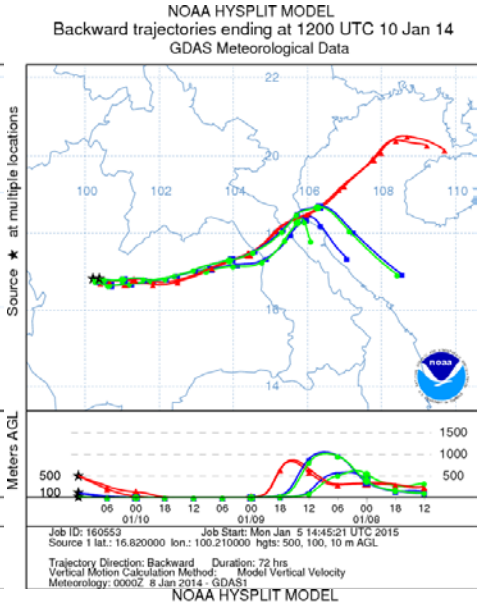
NOAA HYSPLIT MODEL
Backward trajectories ending at 1200 UTC 10 Jan 14
GDAS Meteorological Data
Source ★ at multiple locations
Meters AGL
Job ID: 160553 Job Start: Mon Jan 5 14:45:21 UTC 2015
Source 1 lat.: 16.820000 lon.: 100.210000 hgts: 500, 100, 10 m AGL
Trajectory Direction: Backward Duration: 72 hrs
Vertical Motion Calculation Method: Model Vertical Velocity
Meteorology: 0000Z 8 Jan 2014 - GDAS1

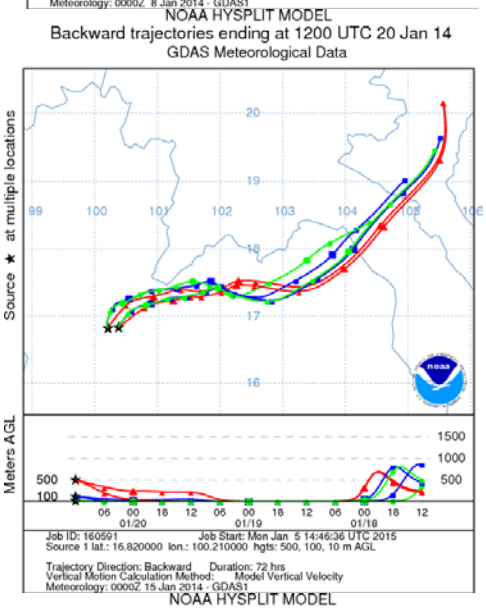
NOAA HYSPLIT MODEL
Backward trajectories ending at 1200 UTC 20 Jan 14
GDAS Meteorological Data
Source ★ at multiple locations
Meters AGL
Job ID: 160591 Job Start: Mon Jan 5 14:46:36 UTC 2015
Source 1 lat.: 16.820000 lon.: 100.210000 hgts: 500, 100, 10 m AGL
Trajectory Direction: Backward Duration: 72 hrs
Vertical Motion Calculation Method: Model Vertical Velocity
Meteorology: 0000Z 15 Jan 2014 - GDAS1

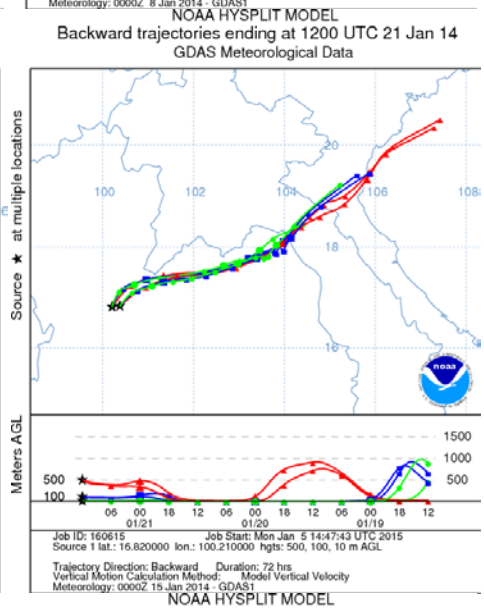
NOAA HYSPLIT MODEL
Backward trajectories ending at 1200 UTC 21 Jan 14
GDAS Meteorological Data
Source ★ at multiple locations
Meters AGL
Job ID: 160615 Job Start: Mon Jan 5 14:47:43 UTC 2015
Source 1 lat.: 16.820000 lon.: 100.210000 hgts: 500, 100, 10 m AGL
Trajectory Direction: Backward Duration: 72 hrs
Vertical Motion Calculation Method: Model Vertical Velocity
Meteorology: 0000Z 15 Jan 2014 - GDAS1

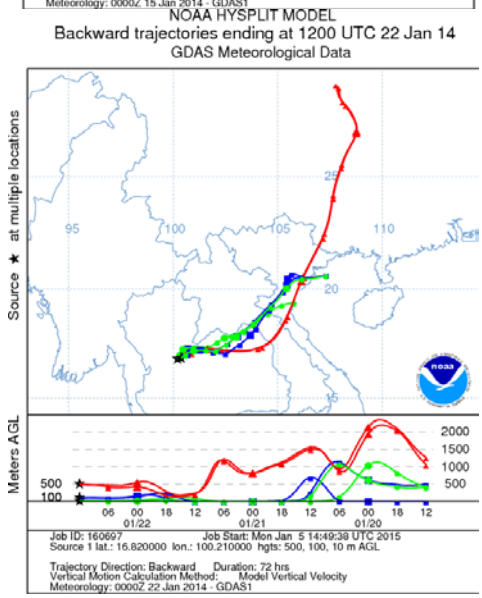
NOAA HYSPLIT MODEL
Backward trajectories ending at 1200 UTC 22 Jan 14
GDAS Meteorological Data
Source ★ at multiple locations
Meters AGL
Job ID: 160697 Job Start: Mon Jan 5 14:49:38 UTC 2015
Source 1 lat.: 16.820000 lon.: 100.210000 hgts: 500, 100, 10 m AGL
Trajectory Direction: Backward Duration: 72 hrs
Vertical Motion Calculation Method: Model Vertical Velocity
Meteorology: 0000Z 22 Jan 2014 - GDAS1

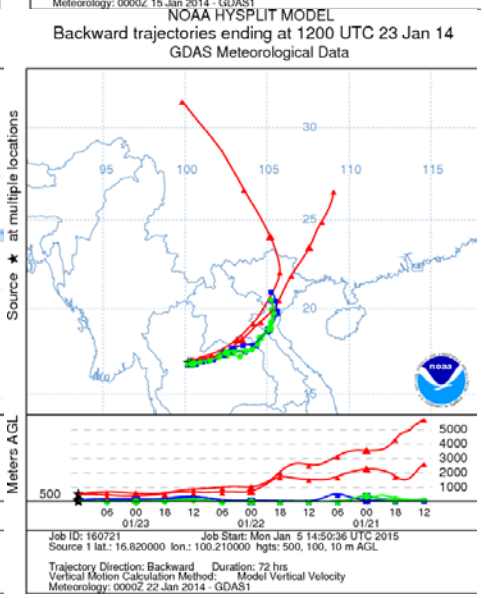
NOAA HYSPLIT MODEL
Backward trajectories ending at 1200 UTC 23 Jan 14
GDAS Meteorological Data
Source ★ at multiple locations
Meters AGL
Job ID: 160721 Job Start: Mon Jan 5 14:50:36 UTC 2015
Source 1 lat.: 16.820000 lon.: 100.210000 hgts: 500, 100, 10 m AGL
Trajectory Direction: Backward Duration: 72 hrs
Vertical Motion Calculation Method: Model Vertical Velocity
Meteorology: 0000Z 22 Jan 2014 - GDAS1

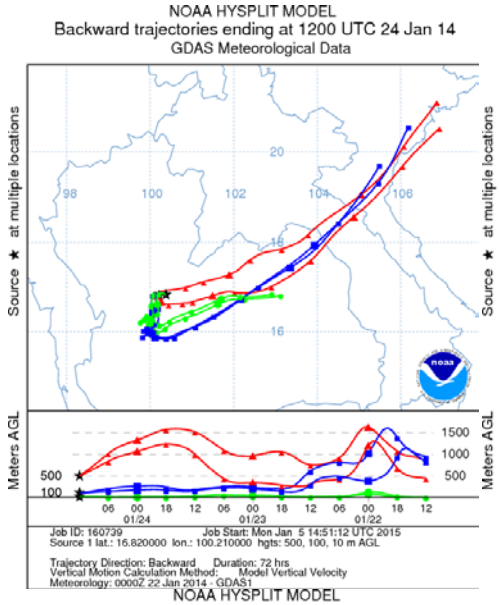
NOAA HYSPLIT MODEL
Backward trajectories ending at 1200 UTC 24 Jan 14
GDAS Meteorological Data
Source ★ at multiple locations
Meters AGL
Job ID: 160739 Job Start: Mon Jan 5 14:51:12 UTC 2015
Source 1 lat.: 16.820000 lon.: 100.210000 hgts: 500, 100, 10 m AGL
Trajectory Direction: Backward Duration: 72 hrs
Vertical Motion Calculation Method: Model Vertical Velocity
Meteorology: 0000Z 22 Jan 2014 - GDAS1

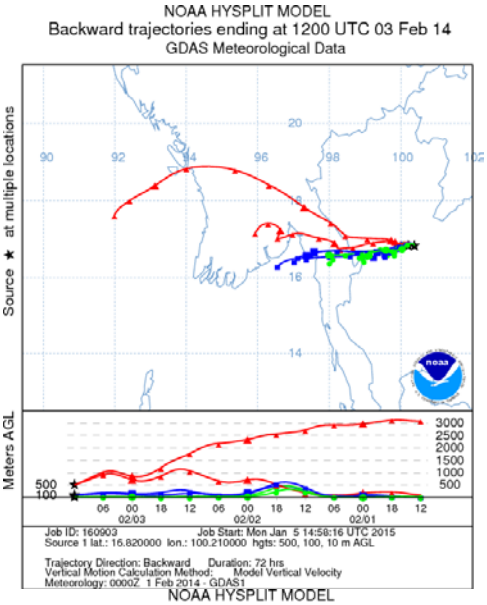
NOAA HYSPLIT MODEL
Backward trajectories ending at 1200 UTC 03 Feb 14
GDAS Meteorological Data
Source ★ at multiple locations
Meters AGL
Job ID: 160902 Job Start: Mon Jan 5 14:58:16 UTC 2015
Source 1 lat.: 16.820000 lon.: 100.210000 hgts: 500, 100, 10 m AGL
Trajectory Direction: Backward Duration: 72 hrs
Vertical Motion Calculation Method: Model Vertical Velocity
Meteorology: 0000Z 1 Feb 2014 - GDAS1

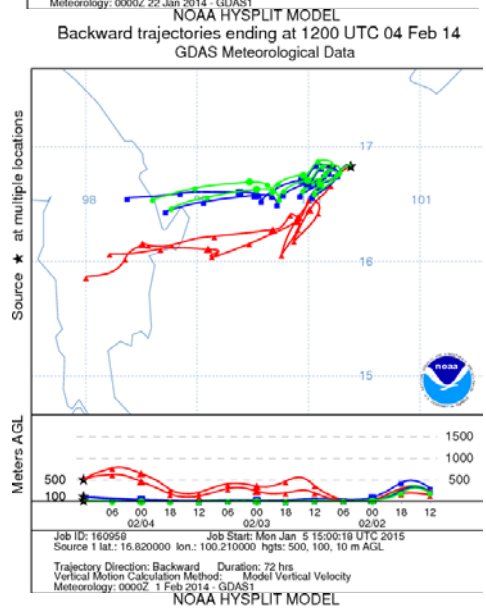
NOAA HYSPLIT MODEL
Backward trajectories ending at 1200 UTC 04 Feb 14
GDAS Meteorological Data
Source ★ at multiple locations
Meters AGL
Job ID: 160958 Job Start: Mon Jan 5 15:00:18 UTC 2015
Source 1 lat.: 16.820000 lon.: 100.210000 hgts: 500, 100, 10 m AGL
Trajectory Direction: Backward Duration: 72 hrs
Vertical Motion Calculation Method: Model Vertical Velocity
Meteorology: 0000Z 1 Feb 2014 - GDAS1

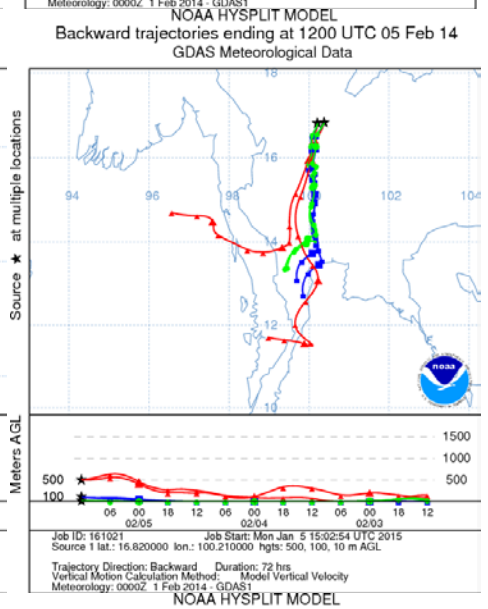
NOAA HYSPLIT MODEL
Backward trajectories ending at 1200 UTC 05 Feb 14
GDAS Meteorological Data
Source ★ at multiple locations
Meters AGL
Job ID: 161021 Job Start: Mon Jan 5 15:02:54 UTC 2015
Source 1 lat.: 16.820000 lon.: 100.210000 hgts: 500, 100, 10 m AGL
Trajectory Direction: Backward Duration: 72 hrs
Vertical Motion Calculation Method: Model Vertical Velocity
Meteorology: 0000Z 1 Feb 2014 - GDAS1

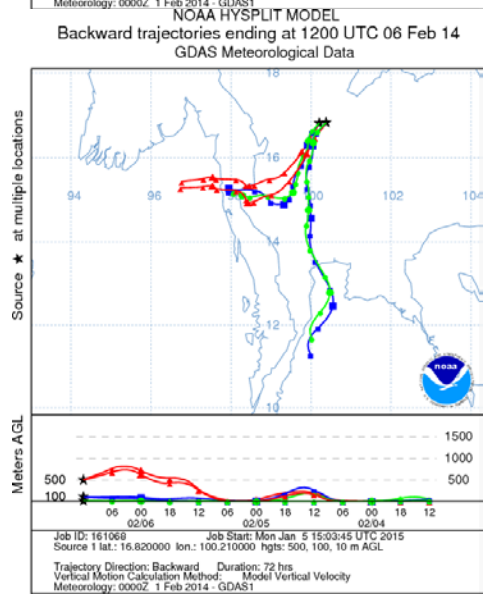
NOAA HYSPLIT MODEL
Backward trajectories ending at 1200 UTC 06 Feb 14
GDAS Meteorological Data
Source ★ at multiple locations
Meters AGL
Job ID: 161069 Job Start: Mon Jan 5 15:03:45 UTC 2015
Source 1 lat.: 16.820000 lon.: 100.210000 hgts: 500, 100, 10 m AGL
Trajectory Direction: Backward Duration: 72 hrs
Vertical Motion Calculation Method: Model Vertical Velocity
Meteorology: 0000Z 1 Feb 2014 - GDAS1

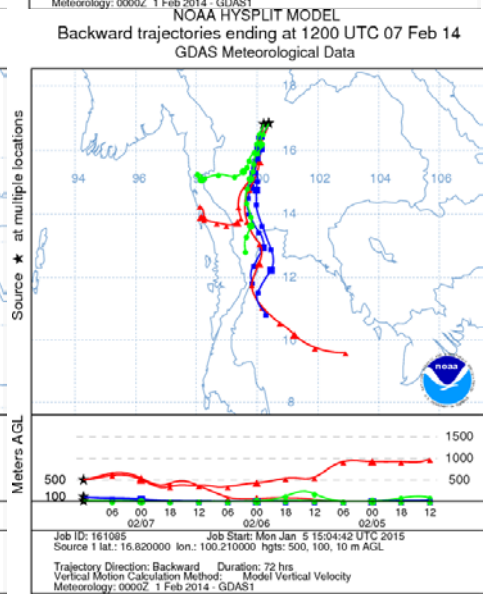
NOAA HYSPLIT MODEL
Backward trajectories ending at 1200 UTC 07 Feb 14
GDAS Meteorological Data
Source ★ at multiple locations
Meters AGL
Job ID: 161085 Job Start: Mon Jan 5 15:04:42 UTC 2015
Source 1 lat.: 16.820000 lon.: 100.210000 hgts: 500, 100, 10 m AGL
Trajectory Direction: Backward Duration: 72 hrs
Vertical Motion Calculation Method: Model Vertical Velocity
Meteorology: 0000Z 1 Feb 2014 - GDAS1

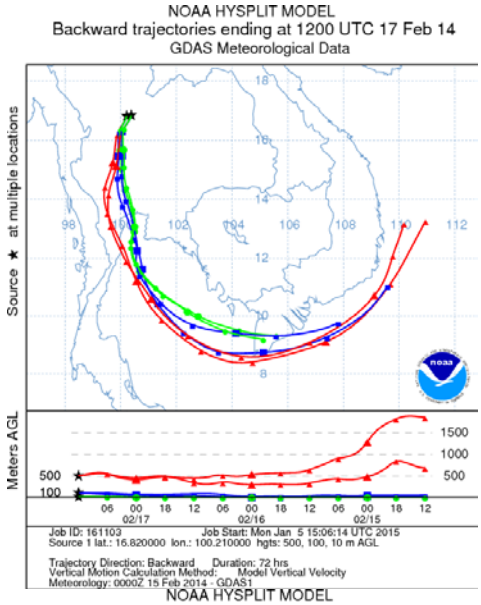
NOAA HYSPLIT MODEL
Backward trajectories ending at 1200 UTC 17 Feb 14
GDAS Meteorological Data
Source ★ at multiple locations
Meters AGL
Job ID: 161103 Job Start: Mon Jan 5 15:06:14 UTC 2015
Source 1 lat.: 16.820000 lon.: 100.210000 hgts: 500, 100, 10 m AGL
Trajectory Direction: Backward Duration: 72 hrs
Vertical Motion Calculation Method: Model Vertical Velocity
Meteorology: 0000Z 15 Feb 2014 - GDAS1

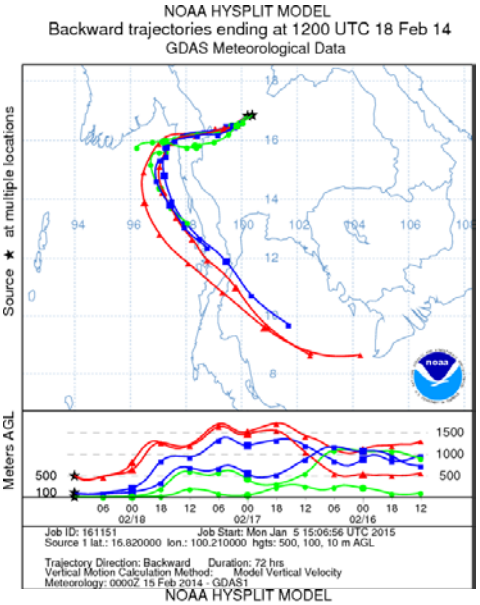
NOAA HYSPLIT MODEL
Backward trajectories ending at 1200 UTC 18 Feb 14
GDAS Meteorological Data
Source ★ at multiple locations
Meters AGL
Job ID: 161151 Job Start: Mon Jan 5 15:06:56 UTC 2015
Source 1 lat.: 16.820000 lon.: 100.210000 hgts: 500, 100, 10 m AGL
Trajectory Direction: Backward Duration: 72 hrs
Vertical Motion Calculation Method: Model Vertical Velocity
Meteorology: 0000Z 15 Feb 2014 - GDAS1

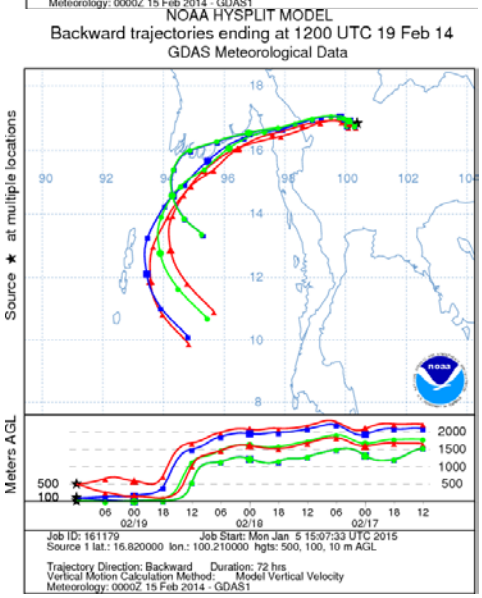
NOAA HYSPLIT MODEL
Backward trajectories ending at 1200 UTC 19 Feb 14
GDAS Meteorological Data
Source ★ at multiple locations
Meters AGL
Job ID: 161179 Job Start: Mon Jan 5 15:07:33 UTC 2015
Source 1 lat.: 16.820000 lon.: 100.210000 hgts: 500, 100, 10 m AGL
Trajectory Direction: Backward Duration: 72 hrs
Vertical Motion Calculation Method: Model Vertical Velocity
Meteorology: 0000Z 15 Feb 2014 - GDAS1

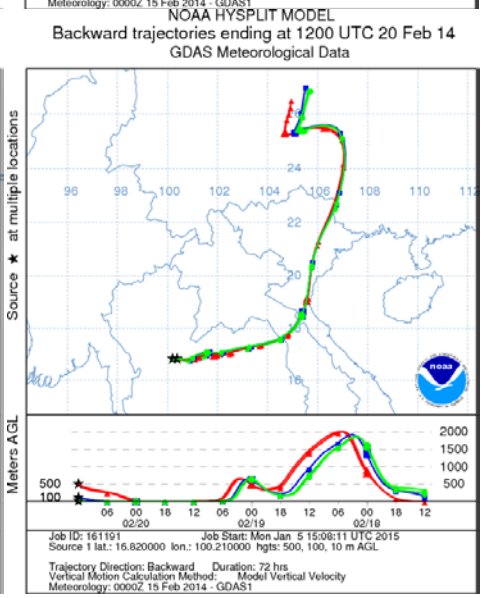
NOAA HYSPLIT MODEL
Backward trajectories ending at 1200 UTC 20 Feb 14
GDAS Meteorological Data
Source ★ at multiple locations
Meters AGL
Job ID: 161191 Job Start: Mon Jan 5 15:08:11 UTC 2015
Source 1 lat.: 16.820000 lon.: 100.210000 hgts: 500, 100, 10 m AGL
Trajectory Direction: Backward Duration: 72 hrs
Vertical Motion Calculation Method: Model Vertical Velocity
Meteorology: 0000Z 15 Feb 2014 - GDAS1

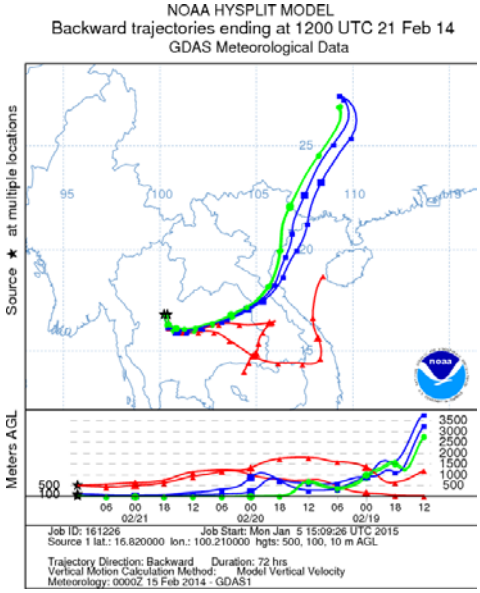
NOAA HYSPLIT MODEL
Backward trajectories ending at 1200 UTC 21 Feb 14
GDAS Meteorological Data
Source ★ at multiple locations
Meters AGL
Job ID: 161226 Job Start: Mon Jan 5 15:09:26 UTC 2015
Source 1 lat.: 16.820000 lon.: 100.210000 hgts: 500, 100, 10 m AGL
Trajectory Direction: Backward Duration: 72 hrs
Vertical Motion Calculation Method: Model Vertical Velocity
Meteorology: 0000Z 15 Feb 2014 - GDAS1

Appendix B

Examples of Trajectory analysis during wet season

(May 2014 – July 2014)

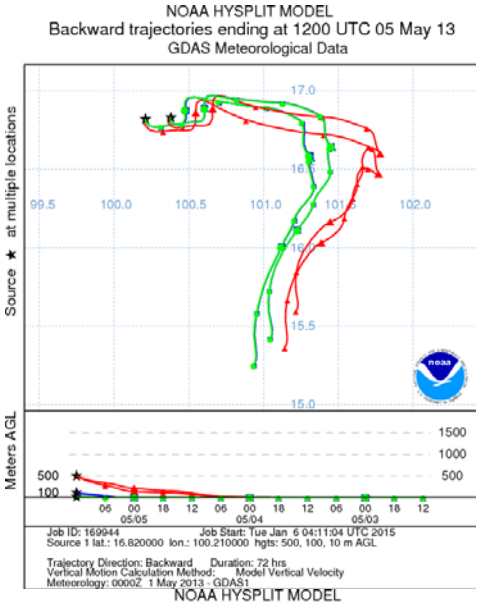
NOAA HYSPLIT MODEL
Backward trajectories ending at 1200 UTC 05 May 13
GDAS Meteorological Data
Source ★ at multiple locations
Meters AGL
Job ID: 169944 Job Start: Tue Jan 6 04:11:04 UTC 2015
Source 1 lat.: 16.820000 lon.: 100.210000 hgts: 500, 100, 10 m AGL
Trajectory Direction: Backward Duration: 72 hrs
Vertical Motion Calculation Method: Model Vertical Velocity
Meteorology: 0000Z 1 May 2013 - GDAS1

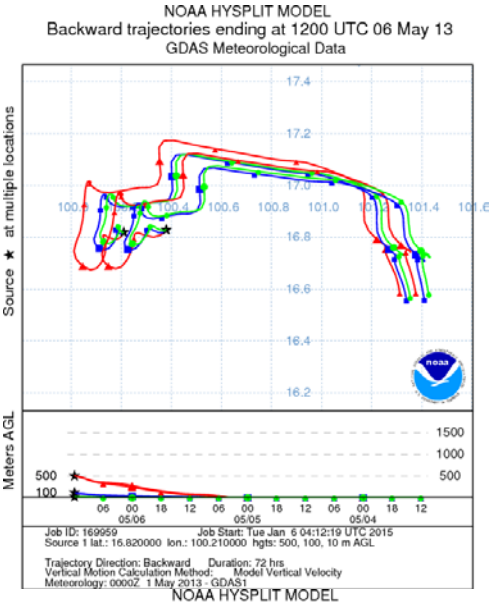
NOAA HYSPLIT MODEL
Backward trajectories ending at 1200 UTC 06 May 13
GDAS Meteorological Data
Source ★ at multiple locations
Meters AGL
Job ID: 169959 Job Start: Tue Jan 6 04:12:19 UTC 2015
Source 1 lat.: 16.820000 lon.: 100.210000 hgts: 500, 100, 10 m AGL
Trajectory Direction: Backward Duration: 72 hrs
Vertical Motion Calculation Method: Model Vertical Velocity
Meteorology: 0000Z 1 May 2013 - GDAS1

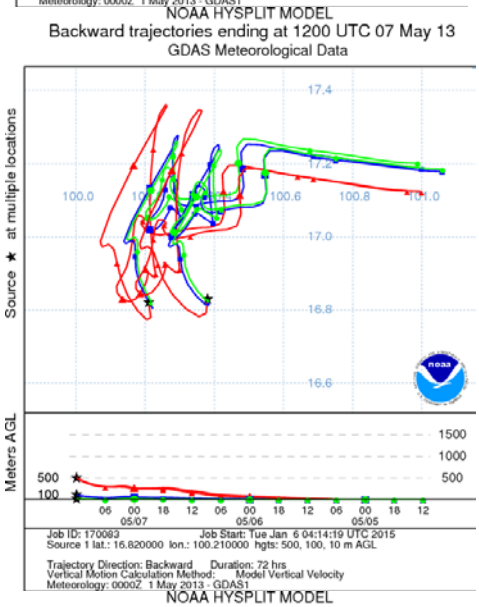
NOAA HYSPLIT MODEL
Backward trajectories ending at 1200 UTC 07 May 13
GDAS Meteorological Data
Source ★ at multiple locations
Meters AGL
Job ID: 170083 Job Start: Tue Jan 6 04:14:19 UTC 2015
Source 1 lat.: 16.820000 lon.: 100.210000 hgts: 500, 100, 10 m AGL
Trajectory Direction: Backward Duration: 72 hrs
Vertical Motion Calculation Method: Model Vertical Velocity
Meteorology: 0000Z 1 May 2013 - GDAS1

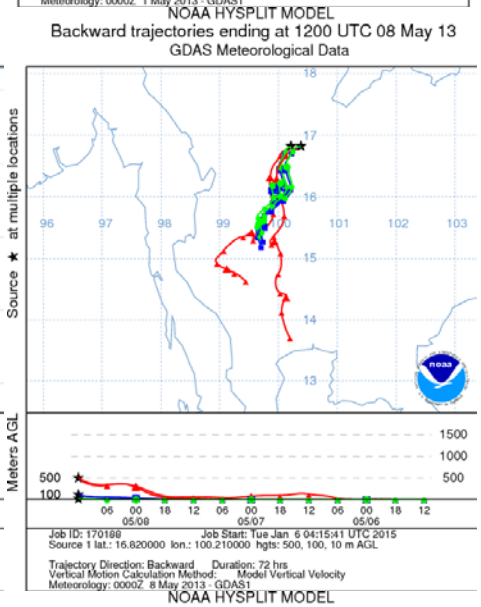
NOAA HYSPLIT MODEL
Backward trajectories ending at 1200 UTC 08 May 13
GDAS Meteorological Data
Source ★ at multiple locations
Meters AGL
Job ID: 170188 Job Start: Tue Jan 6 04:15:41 UTC 2015
Source 1 lat.: 16.820000 lon.: 100.210000 hgts: 500, 100, 10 m AGL
Trajectory Direction: Backward Duration: 72 hrs
Vertical Motion Calculation Method: Model Vertical Velocity
Meteorology: 0000Z 8 May 2013 - GDAS1

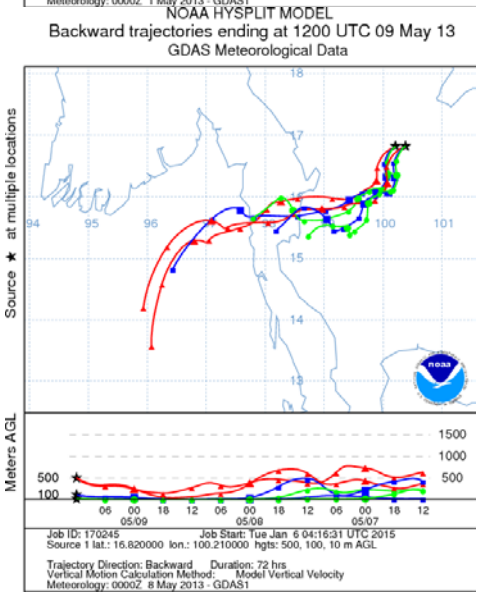
NOAA HYSPLIT MODEL
Backward trajectories ending at 1200 UTC 09 May 13
GDAS Meteorological Data
Source ★ at multiple locations
Meters AGL
Job ID: 170245 Job Start: Tue Jan 6 04:16:31 UTC 2015
Source 1 lat.: 16.820000 lon.: 100.210000 hgts: 500, 100, 10 m AGL
Trajectory Direction: Backward Duration: 72 hrs
Vertical Motion Calculation Method: Model Vertical Velocity
Meteorology: 0000Z 8 May 2013 - GDAS1

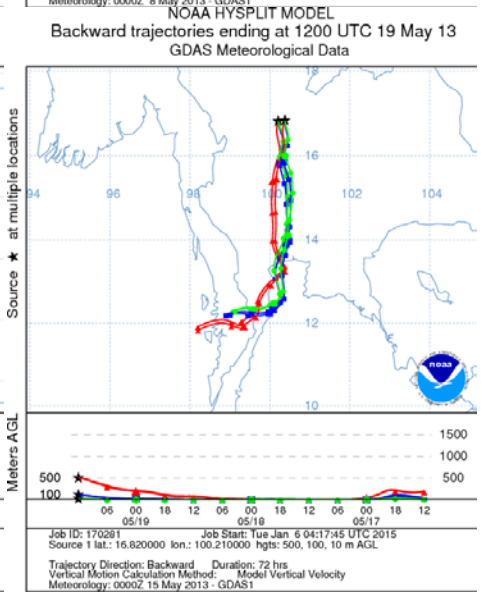
NOAA HYSPLIT MODEL
Backward trajectories ending at 1200 UTC 19 May 13
GDAS Meteorological Data
Source ★ at multiple locations
Meters AGL
Job ID: 170281 Job Start: Tue Jan 6 04:17:45 UTC 2015
Source 1 lat.: 16.820000 lon.: 100.210000 hgts: 500, 100, 10 m AGL
Trajectory Direction: Backward Duration: 72 hrs
Vertical Motion Calculation Method: Model Vertical Velocity
Meteorology: 0000Z 15 May 2013 - GDAS1

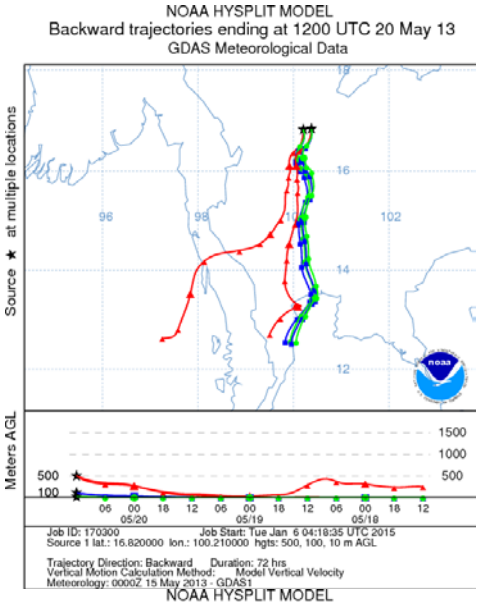
NOAA HYSPLIT MODEL
Backward trajectories ending at 1200 UTC 20 May 13
GDAS Meteorological Data
Source ★ at multiple locations
Meters AGL
Job ID: 170300 Job Start: Tue Jan 6 04:18:35 UTC 2015
Source 1 lat.: 16.820000 lon.: 100.210000 hgts: 500, 100, 10 m AGL
Trajectory Direction: Backward Duration: 72 hrs
Vertical Motion Calculation Method: Model Vertical Velocity
Meteorology: 0000Z 15 May 2013 - GDAS1

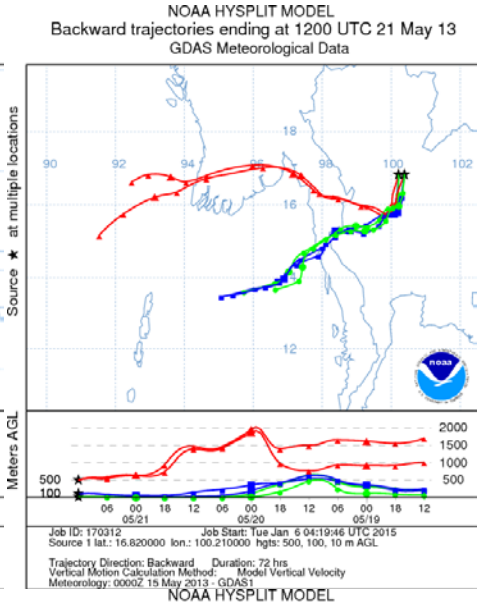
NOAA HYSPLIT MODEL
Backward trajectories ending at 1200 UTC 21 May 13
GDAS Meteorological Data
Source ★ at multiple locations
Meters AGL
Job ID: 170312 Job Start: Tue Jan 6 04:19:46 UTC 2015
Source 1 lat.: 16.820000 lon.: 100.210000 hgts: 500, 100, 10 m AGL
Trajectory Direction: Backward Duration: 72 hrs
Vertical Motion Calculation Method: Model Vertical Velocity
Meteorology: 0000Z 15 May 2013 - GDAS1

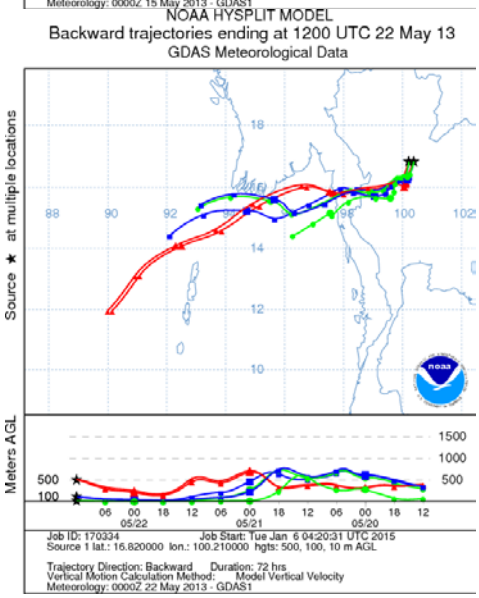
NOAA HYSPLIT MODEL
Backward trajectories ending at 1200 UTC 22 May 13
GDAS Meteorological Data
Source ★ at multiple locations
Meters AGL
Job ID: 170334 Job Start: Tue Jan 6 04:20:31 UTC 2015
Source 1 lat.: 16.820000 lon.: 100.210000 hgts: 500, 100, 10 m AGL
Trajectory Direction: Backward Duration: 72 hrs
Vertical Motion Calculation Method: Model Vertical Velocity
Meteorology: 0000Z 22 May 2013 - GDAS1

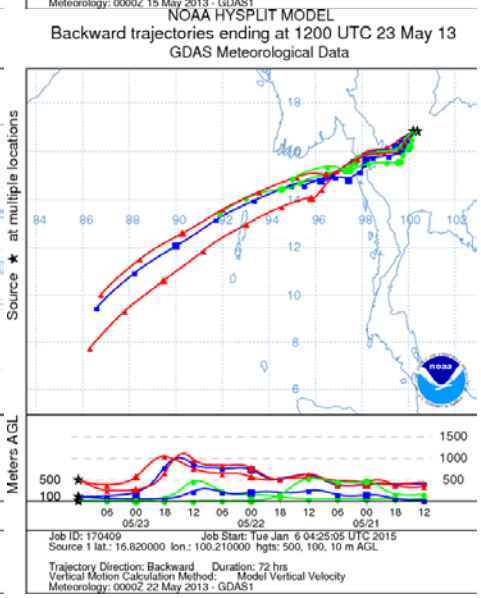
NOAA HYSPLIT MODEL
Backward trajectories ending at 1200 UTC 23 May 13
GDAS Meteorological Data
Source ★ at multiple locations
Meters AGL
Job ID: 170409 Job Start: Tue Jan 6 04:25:05 UTC 2015
Source 1 lat.: 16.820000 lon.: 100.210000 hgts: 500, 100, 10 m AGL
Trajectory Direction: Backward Duration: 72 hrs
Vertical Motion Calculation Method: Model Vertical Velocity
Meteorology: 0000Z 22 May 2013 - GDAS1

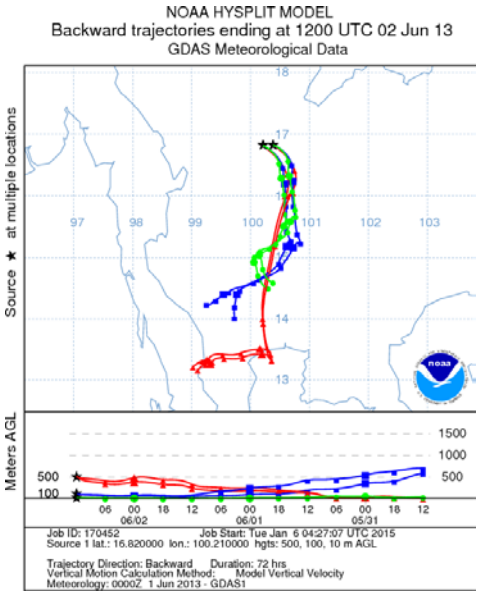
NOAA HYSPLIT MODEL
Backward trajectories ending at 1200 UTC 02 Jun 13
GDAS Meteorological Data
Source ★ at multiple locations
Meters AGL
Job ID: 170452 Job Start: Tue Jan 6 04:27:07 UTC 2015
Source 1 lat.: 16.820000 lon.: 100.210000 hgts: 500, 100, 10 m AGL
Trajectory Direction: Backward Duration: 72 hrs
Vertical Motion Calculation Method: Model Vertical Velocity
Meteorology: 0000Z 1 Jun 2013 - GDAS1

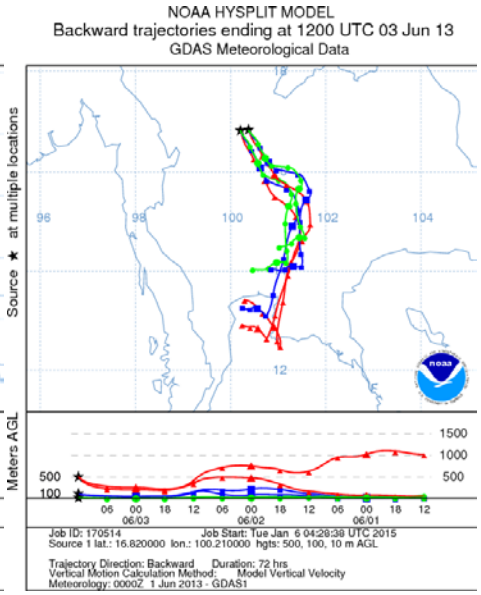
NOAA HYSPLIT MODEL
Backward trajectories ending at 1200 UTC 03 Jun 13
GDAS Meteorological Data
Source ★ at multiple locations
Meters AGL
Job ID: 170514 Job Start: Tue Jan 6 04:28:38 UTC 2015
Source 1 lat.: 16.820000 lon.: 100.210000 hgts: 500, 100, 10 m AGL
Trajectory Direction: Backward Duration: 72 hrs
Vertical Motion Calculation Method: Model Vertical Velocity
Meteorology: 0000Z 1 Jun 2013 - GDAS1

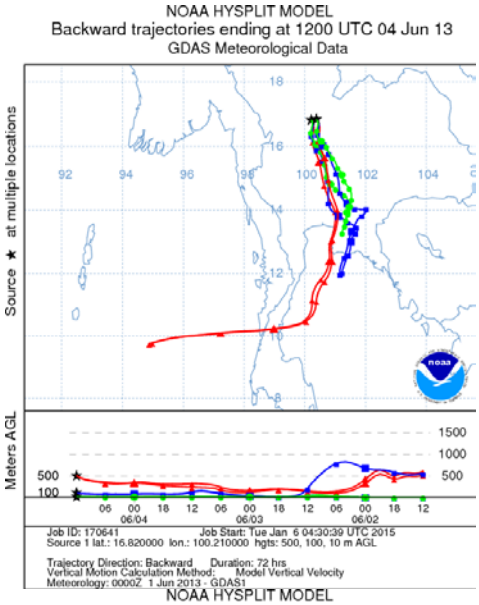
NOAA HYSPLIT MODEL
Backward trajectories ending at 1200 UTC 04 Jun 13
GDAS Meteorological Data
Source ★ at multiple locations
Meters AGL
Job ID: 170641 Job Start: Tue Jan 6 04:30:39 UTC 2015
Source 1 lat.: 16.820000 lon.: 100.210000 hgts: 500, 100, 10 m AGL
Trajectory Direction: Backward Duration: 72 hrs
Vertical Motion Calculation Method: Model Vertical Velocity
Meteorology: 0000Z 1 Jun 2013 - GDAS1

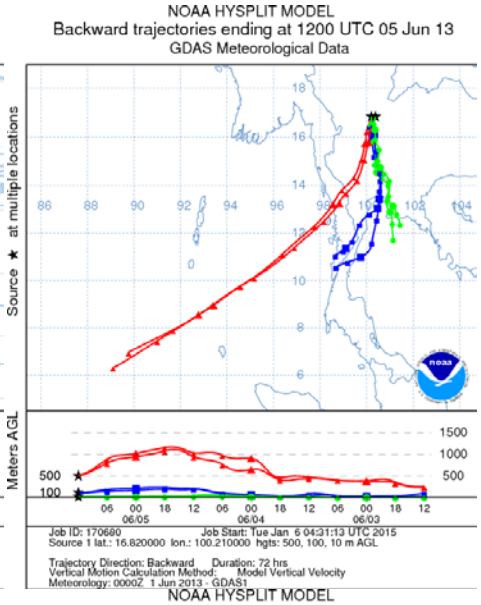
NOAA HYSPLIT MODEL
Backward trajectories ending at 1200 UTC 05 Jun 13
GDAS Meteorological Data
Source ★ at multiple locations
Meters AGL
Job ID: 170680 Job Start: Tue Jan 6 04:31:13 UTC 2015
Source 1 lat.: 16.820000 lon.: 100.210000 hgts: 500, 100, 10 m AGL
Trajectory Direction: Backward Duration: 72 hrs
Vertical Motion Calculation Method: Model Vertical Velocity
Meteorology: 0000Z 1 Jun 2013 - GDAS1

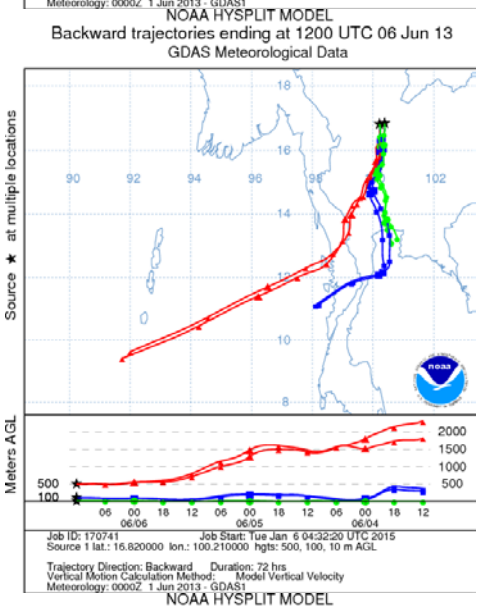
NOAA HYSPLIT MODEL
Backward trajectories ending at 1200 UTC 06 Jun 13
GDAS Meteorological Data
Source ★ at multiple locations
Meters AGL
Job ID: 170741 Job Start: Tue Jan 6 04:32:20 UTC 2015
Source 1 lat.: 16.820000 lon.: 100.210000 hgts: 500, 100, 10 m AGL
Trajectory Direction: Backward Duration: 72 hrs
Vertical Motion Calculation Method: Model Vertical Velocity
Meteorology: 0000Z 1 Jun 2013 - GDAS1

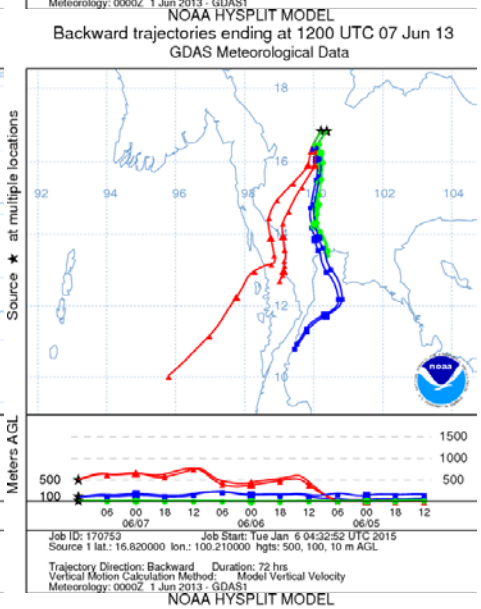
NOAA HYSPLIT MODEL
Backward trajectories ending at 1200 UTC 07 Jun 13
GDAS Meteorological Data
Source ★ at multiple locations
Meters AGL
Job ID: 170753 Job Start: Tue Jan 6 04:32:52 UTC 2015
Source 1 lat.: 16.820000 lon.: 100.210000 hgts: 500, 100, 10 m AGL
Trajectory Direction: Backward Duration: 72 hrs
Vertical Motion Calculation Method: Model Vertical Velocity
Meteorology: 0000Z 1 Jun 2013 - GDAS1

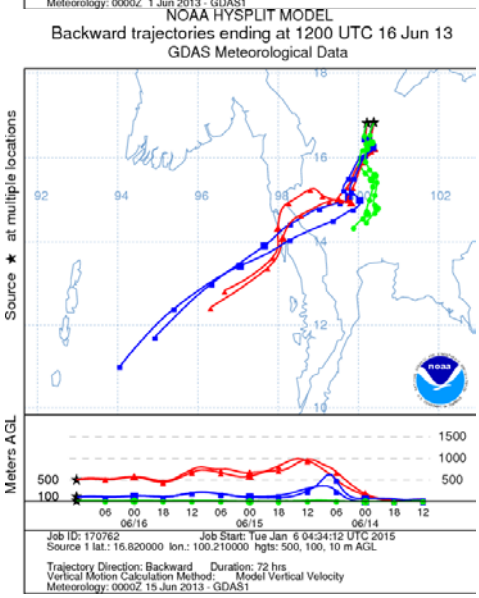
NOAA HYSPLIT MODEL
Backward trajectories ending at 1200 UTC 16 Jun 13
GDAS Meteorological Data
Source ★ at multiple locations
Meters AGL
Job ID: 170762 Job Start: Tue Jan 6 04:34:12 UTC 2015
Source 1 lat.: 16.820000 lon.: 100.210000 hgts: 500, 100, 10 m AGL
Trajectory Direction: Backward Duration: 72 hrs
Vertical Motion Calculation Method: Model Vertical Velocity
Meteorology: 0000Z 15 Jun 2013 - GDAS1

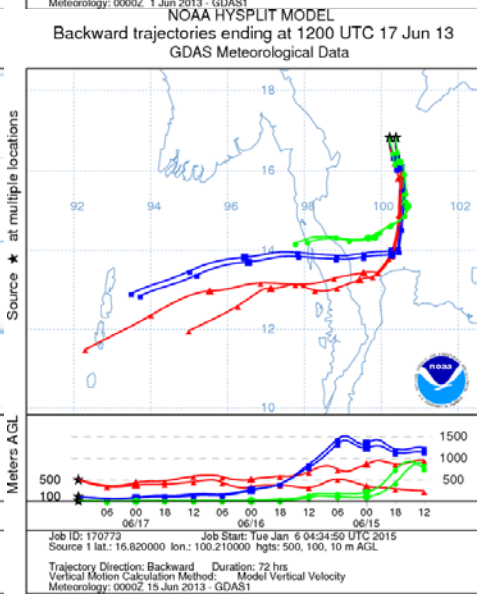
NOAA HYSPLIT MODEL
Backward trajectories ending at 1200 UTC 17 Jun 13
GDAS Meteorological Data
Source ★ at multiple locations
Meters AGL
Job ID: 170773 Job Start: Tue Jan 6 04:34:50 UTC 2015
Source 1 lat.: 16.820000 lon.: 100.210000 hgts: 500, 100, 10 m AGL
Trajectory Direction: Backward Duration: 72 hrs
Vertical Motion Calculation Method: Model Vertical Velocity
Meteorology: 0000Z 15 Jun 2013 - GDAS1

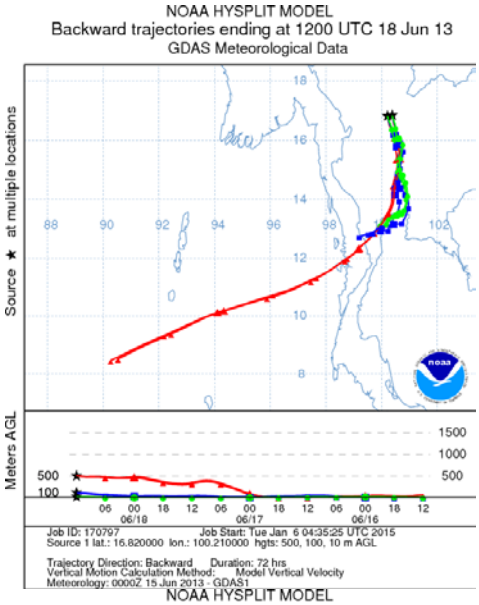
NOAA HYSPLIT MODEL
Backward trajectories ending at 1200 UTC 18 Jun 13
GDAS Meteorological Data
Source ★ at multiple locations
Meters AGL
Job ID: 170707 Job Start: Tue Jan 6 04:35:25 UTC 2015
Source 1 lat.: 16.820000 lon.: 100.210000 hgts: 500, 100, 10 m AGL
Trajectory Direction: Backward Duration: 72 hrs
Vertical Motion Calculation Method: Model Vertical Velocity
Meteorology: 0000Z 15 Jun 2013 - GDAS1

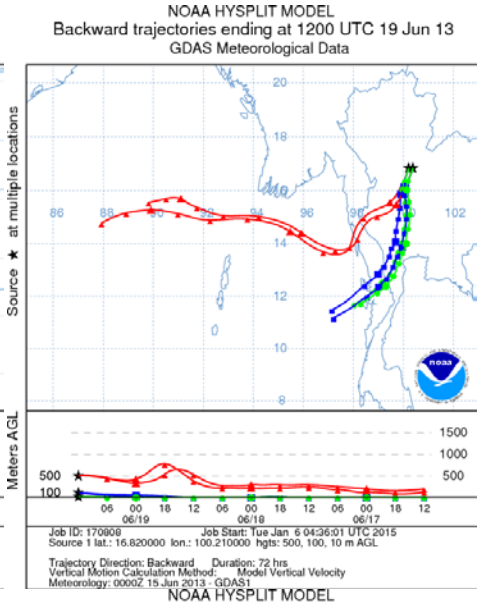
NOAA HYSPLIT MODEL
Backward trajectories ending at 1200 UTC 19 Jun 13
GDAS Meteorological Data
Source ★ at multiple locations
Meters AGL
Job ID: 170808 Job Start: Tue Jan 6 04:36:01 UTC 2015
Source 1 lat.: 16.820000 lon.: 100.210000 hgts: 500, 100, 10 m AGL
Trajectory Direction: Backward Duration: 72 hrs
Vertical Motion Calculation Method: Model Vertical Velocity
Meteorology: 0000Z 15 Jun 2013 - GDAS1

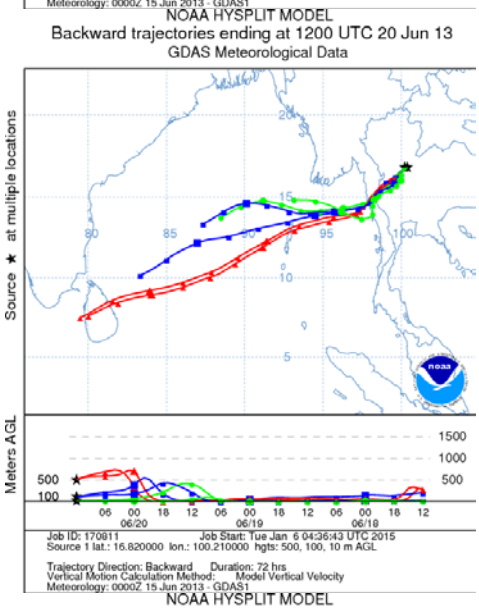
NOAA HYSPLIT MODEL
Backward trajectories ending at 1200 UTC 20 Jun 13
GDAS Meteorological Data
Source ★ at multiple locations
Meters AGL
Job ID: 170911 Job Start: Tue Jan 6 04:36:43 UTC 2015
Source 1 lat.: 16.820000 lon.: 100.210000 hgts: 500, 100, 10 m AGL
Trajectory Direction: Backward Duration: 72 hrs
Vertical Motion Calculation Method: Model Vertical Velocity
Meteorology: 0000Z 15 Jun 2013 - GDAS1

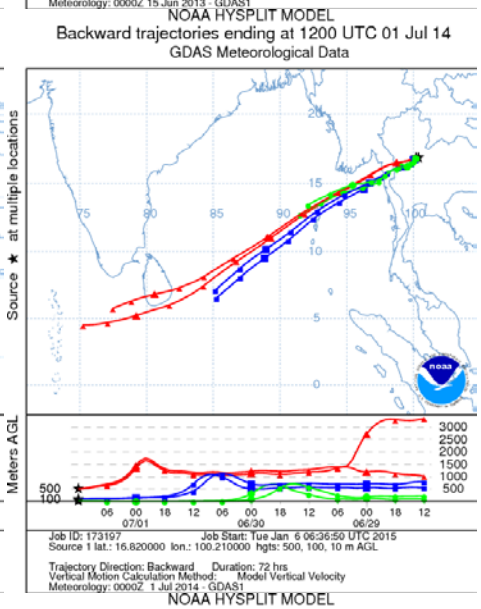
NOAA HYSPLIT MODEL
Backward trajectories ending at 1200 UTC 01 Jul 14
GDAS Meteorological Data
Source ★ at multiple locations
Meters AGL
Job ID: 173197 Job Start: Tue Jan 6 06:36:50 UTC 2015
Source 1 lat.: 16.820000 lon.: 100.210000 hgts: 500, 100, 10 m AGL
Trajectory Direction: Backward Duration: 72 hrs
Vertical Motion Calculation Method: Model Vertical Velocity
Meteorology: 0000Z 1 Jul 2014 - GDAS1

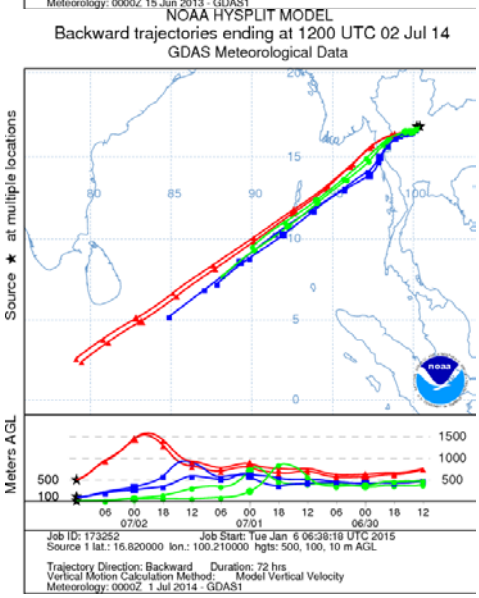
NOAA HYSPLIT MODEL
Backward trajectories ending at 1200 UTC 02 Jul 14
GDAS Meteorological Data
Source ★ at multiple locations
Meters AGL
Job ID: 173252 Job Start: Tue Jan 6 06:38:18 UTC 2015
Source 1 lat.: 16.820000 lon.: 100.210000 hgts: 500, 100, 10 m AGL
Trajectory Direction: Backward Duration: 72 hrs
Vertical Motion Calculation Method: Model Vertical Velocity
Meteorology: 0000Z 1 Jul 2014 - GDAS1

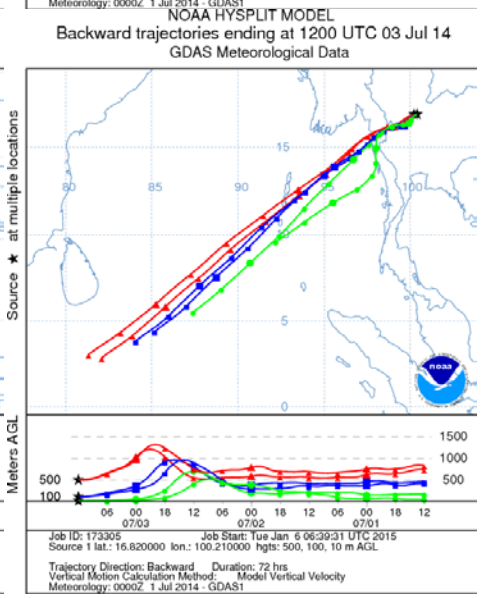
NOAA HYSPLIT MODEL
Backward trajectories ending at 1200 UTC 03 Jul 14
GDAS Meteorological Data
Source ★ at multiple locations
Meters AGL
Job ID: 173305 Job Start: Tue Jan 6 06:39:31 UTC 2015
Source 1 lat.: 16.820000 lon.: 100.210000 hgts: 500, 100, 10 m AGL
Trajectory Direction: Backward Duration: 72 hrs
Vertical Motion Calculation Method: Model Vertical Velocity
Meteorology: 0000Z 1 Jul 2014 - GDAS1

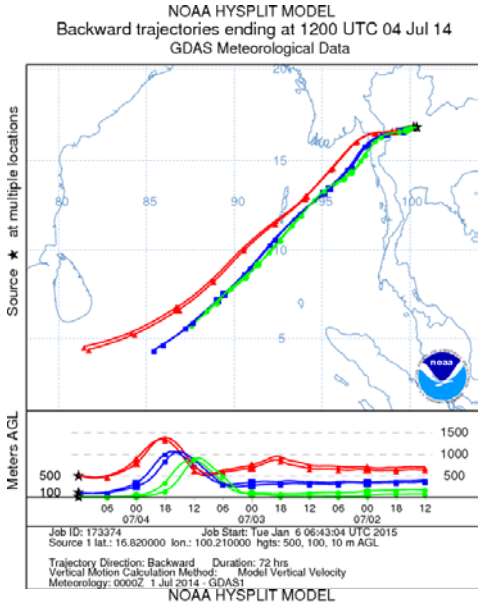
NOAA HYSPLIT MODEL
Backward trajectories ending at 1200 UTC 04 Jul 14
GDAS Meteorological Data
Source ★ at multiple locations
Meters AGL
Job ID: 173374 Job Start: Tue Jan 6 06:43:04 UTC 2015
Source 1 lat.: 16.820000 lon.: 100.210000 hgts: 500, 100, 10 m AGL
Trajectory Direction: Backward Duration: 72 hrs
Vertical Motion Calculation Method: Model Vertical Velocity
Meteorology: 0000Z 1 Jul 2014 - GDAS1

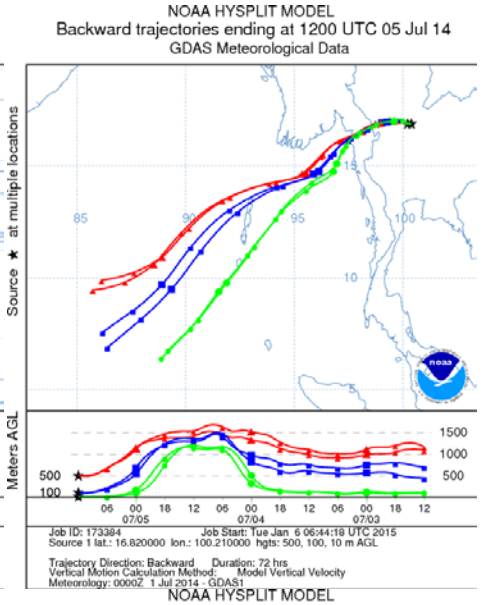
NOAA HYSPLIT MODEL
Backward trajectories ending at 1200 UTC 05 Jul 14
GDAS Meteorological Data
Source ★ at multiple locations
Meters AGL
Job ID: 173384 Job Start: Tue Jan 6 06:44:18 UTC 2015
Source 1 lat.: 16.820000 lon.: 100.210000 hgts: 500, 100, 10 m AGL
Trajectory Direction: Backward Duration: 72 hrs
Vertical Motion Calculation Method: Model Vertical Velocity
Meteorology: 0000Z 1 Jul 2014 - GDAS1

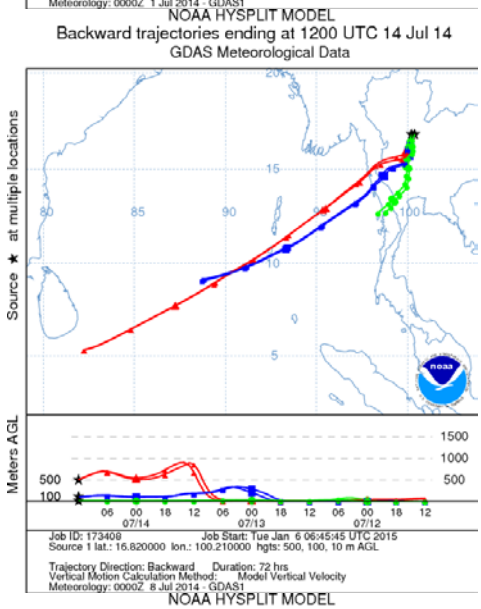
NOAA HYSPLIT MODEL
Backward trajectories ending at 1200 UTC 14 Jul 14
GDAS Meteorological Data
Source ★ at multiple locations
Meters AGL
Job ID: 173408 Job Start: Tue Jan 6 06:45:45 UTC 2015
Source 1 lat.: 16.820000 lon.: 100.210000 hgts: 500, 100, 10 m AGL
Trajectory Direction: Backward Duration: 72 hrs
Vertical Motion Calculation Method: Model Vertical Velocity
Meteorology: 0000Z 8 Jul 2014 - GDAS1

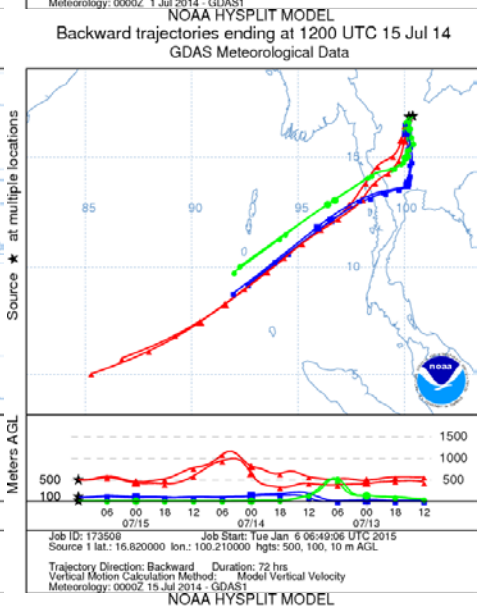
NOAA HYSPLIT MODEL
Backward trajectories ending at 1200 UTC 15 Jul 14
GDAS Meteorological Data
Source ★ at multiple locations
Meters AGL
Job ID: 173508 Job Start: Tue Jan 6 06:49:06 UTC 2015
Source 1 lat.: 16.820000 lon.: 100.210000 hgts: 500, 100, 10 m AGL
Trajectory Direction: Backward Duration: 72 hrs
Vertical Motion Calculation Method: Model Vertical Velocity
Meteorology: 0000Z 15 Jul 2014 - GDAS1

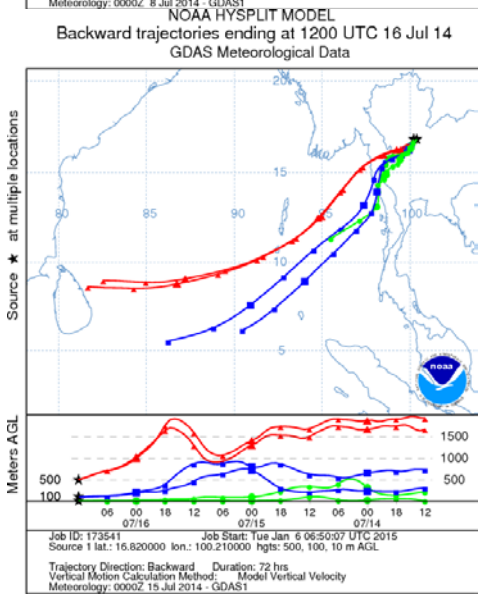
NOAA HYSPLIT MODEL
Backward trajectories ending at 1200 UTC 16 Jul 14
GDAS Meteorological Data
Source ★ at multiple locations
Meters AGL
Job ID: 173541 Job Start: Tue Jan 6 06:50:07 UTC 2015
Source 1 lat.: 16.820000 lon.: 100.210000 hgts: 500, 100, 10 m AGL
Trajectory Direction: Backward Duration: 72 hrs
Vertical Motion Calculation Method: Model Vertical Velocity
Meteorology: 0000Z 15 Jul 2014 - GDAS1

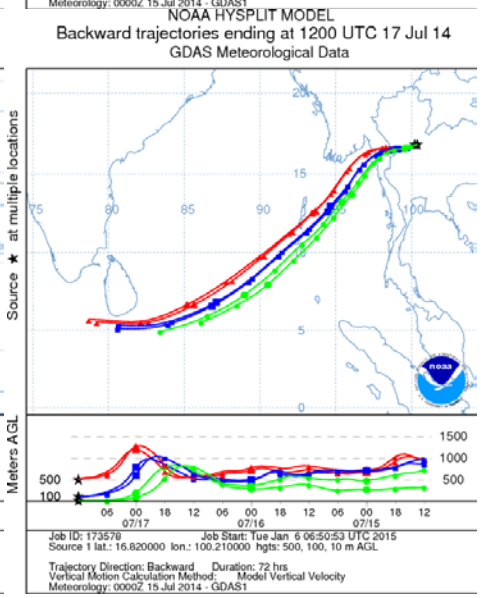
NOAA HYSPLIT MODEL
Backward trajectories ending at 1200 UTC 17 Jul 14
GDAS Meteorological Data
Source ★ at multiple locations
Meters AGL
Job ID: 173578 Job Start: Tue Jan 6 06:50:53 UTC 2015
Source 1 lat.: 16.820000 lon.: 100.210000 hgts: 500, 100, 10 m AGL
Trajectory Direction: Backward Duration: 72 hrs
Vertical Motion Calculation Method: Model Vertical Velocity
Meteorology: 0000Z 15 Jul 2014 - GDAS1